NASA CONTRACTOR REPORT

NASA CR-54009

N64-17222
CODE-1

NASA CR-54009

VAPOR-FILLED THERMIONIC CONVERTERS

by K. G. Hernqvist, J. R. Fendley, H. Hendel, J. D. Levine, and P. Rappaport

OTS PRICE
XEROX $
MICROFILM $

FINAL REPORT

Prepared under Contract No. NAS 3-2531

RADIO CORPORATION OF AMERICA
RCA LABORATORIES
PRINCETON, NEW JERSEY

for

NATIONAL AERONAUTICS & SPACE ADMINISTRATION • WASHINGTON, D. C. • December 1963

NASA CONTRACTOR REPORT

(NASA CR-54009)

NASA CR-54009

OTS: $5.60 ph, $1.85 mf

N64 17222

Code-1

VAPOR-FILLED THERMIONIC CONVERTERS

Prepared by K. G. Hernqvist, ~~Project Engineer~~, J. R. Fendley, H. Hendel, and J. D. Levine

Dec. 1963 55p nfa

Approved by P. Rappaport, Project Supervisor

FINAL REPORT

2 Prepared (NASA) under Contract No. NAS 3-2531

(1916642)

RADIO CORPORATION OF AMERICA
RCA LABORATORIES
PRINCETON, NEW JERSEY

for

NATIONAL AERONAUTICS & SPACE ADMINISTRATION • WASHINGTON, D. C. • December 1963

TABLE OF CONTENTS

TABLE OF CONTENTS (Continued)

LIST OF ILLUSTRATIONS

GLOSSARY OF TERMS

A	Conversion factor
A_{xe}	Mass of the atom
C	Circumference
D	Dose rate in Roentgen units
E	Energy of incident photon
$E_a(\theta, T)$	Atom desorption rate
$E_p(\theta, T)$	$\exp(-\phi_x/kT)$ Net ion transmission rate
$E'(T')$	Arrival rate
e	Electronic charge
H	Magnetic field in gauss
h	Planck's constant
$I_e(T, T', \phi_x)$	Electron emission
J_g	Number of ions produced per unit mass
j_e	Electron current density in A/cm^2
k	Boltzmann's constant
L	Length
m	Mass of one cesium atom
m_e	Mass of one electron
N	Number of ions/cm^3
n	Number of electrons/gram
n_+	Number of ions/cm^2/sec
n_{xe}	Number of atoms/cm^3 of diode gap
R	Total dose in Roentgens
T	Surface temperature (also, kinetic energy)
T′	Vapor bath temperature
W	Energy necessary to produce an ion-electron pair in the gas
δ	Compton absorption coefficient
$\Delta S(\theta)$	Configuration entropy change
θ	Coverage
K	Pair production absorption coefficient
μ_a	Linear absorption coefficient
ν, ν'	Vibration frequencies
ρ	Density
σ_f, σ'	Surface densities of monolayers
τ	Photoelectric absorption coefficient
Φ	Binding energy of electron
ϕ'	Heat of vaporization
ϕ_a	Heat of adsorption
ϕ_{ao}	Calculated adsorption heat at $\theta = 0$
ϕ_e	Electron work function of the partially coated surface
$\phi_a(\theta)$	Atom desorption heat
ϕ_{po}	For desorption energy
ϕ_x	Applied electrostatic potential
ω_a	Statistical weight for atoms
ω_p	Statistical weight for ions

ABSTRACT

First, electron emission S-curves are computer-calculated by means of the Levine-Gyftopoulos adsorption theory, using no adjustable parameters. Predictions are made for cesium on various crystal faces and on 21 transition metals. Comparison with available experimental data is good.

A simplified appropriate treatment of adsorption theory is given. It is shown that a new dimensionless parameter characterizes, to a first approximation, electron emission S-curve performance for different adsorbates, substrates, and arrival dates.

A recently initiated study of cesium adsorption on insulators has been carried out both theoretically and experimentally. Among other things, it is discovered that the cesium is adsorbed on an insulator as a molecular ion with a binding energy of 1.65 ev.

An analysis of the cesium vapor arc discharge is presented.

Apparatus is described which permits continuous pumping of cesium vapor devices. Using this apparatus, the outgassing from an operating cesium diode has been analyzed, and typical results are presented.

Experimental data on the results of dosing an arc mode cesium diode with xenon and krypton are given, and a discussion of these results is included. Finally, a study is made which predicts the effect of nuclear reactor radiation on a cesium diode dosed with xenon gas.

Author

INTRODUCTION

An idealized thermionic converter is a device consisting of electrodes, ceramic insulators, and cesium vapor. For a complete understanding of the electrical performance of such a device, a detailed knowledge is required of the interaction of cesium with metal surfaces and insulators, as well as the role played by cesium in plasma generation and electron transport through the interelectrode space. Research in all of these areas is described in this report. It is shown that electron emission properties of cesium-covered metals can be calculated based solely on fundamental properties of the adsorbate and the substrate. Newly initiated research on cesium-covered ceramics has advanced the understanding of interaction between cesium and insulators. It is shown that the ball-of-fire analysis of the cesium arc gives a qualitative understanding of cesium plasma generation and electron transport properties of the plasma. Knowledge of fundamental interaction cross sections for cesium is needed for a quantitative prediction of the converter performance.

In practical converters additional substances are present in the gas phase, on the electrodes, or both. Such substances, although present in minute quantities, can have profound effects on the performance of the converter. These additives can be inadvertently carried into the converter or they may be purposely added for specific purposes. In either case, an understanding of their effects and a know-how of their control is of paramount importance for the operation of thermionic converters. This report describes research on analysis of impurities evolving in converters and effects of purposely added noble gases on converter performance.

I. COMPUTER CALCULATIONS OF ELECTRON EMISSIONS-CURVES

by
Jules D. Levine

A. INTRODUCTION

In a previous study[1] and in studies soon to be published[2-4] theoretical expressions are derived for important properties of the adsorption system of metals partially coated by metallic particles. These properties are the electron work function, heat of adsorption, rate of desorption, and equation of state. No adjustables appear in the theoretical equations – only known parameters, characteristic of pure adsorbate and pure substrate materials, are used.

By suitably combining these properties, electron emission S-curves can be constructed as indicated in ref. 4. But the procedure is extremely laborious when attempted by hand calculation. Therefore, a computer program was initiated and run at the RCA Laboratories using an IBM 650 computer to facilitate the calculations. The scope of the computer calculations allows new conclusions to be drawn which would not be possible from the necessarily limited hand-calculated data.

The object of this study is to investigate S-curves for cesium adsorbed on different substrate crystal faces and at different bath temperatures. Rasor[5] has been able to predict electron emission from Cs on transition metals by using a perturbation study of the Taylor-Langmuir[6] Cs-W system. Danforth[7] has predicted kinetics of electron emission from Th on W, but he requires the initial heat of adsorption as an adjustable parameter.

But the outstanding characteristic of this section is that no adjustables or reference systems are required. Also, no new physics is required since the main concepts and supporting equations are, or will be, reported elsewhere.[1-4] These concepts and equations are general in the sense that they apply to many metallic adsorbates and substrates, and over large ranges of coverage, surface temperature, and bath temperature.

To solve the theoretical equations, certain input parameters must be specified. Some are characteristic of the bulk properties of pure absorbate and substrate: heat of sublimation, bare electron work function, covalent radius, and Pauling angular strength.[4] The others are characteristic of adsorbate above: ionization potential, valence, liquid density, and polarizability. Although typical values of these parameters are given in Table 1 of ref. 2 and Table 1 of ref. 3 for 21 substrates and 13 adsorbates, it is recognized that the electron work function of the bare metal ϕ_m, electron work function of epitaxially grown bulk adsorbate ϕ_f, and adsorbate density at one monolayer σ_f are very sensitive to crystal face. These three input parameters should, therefore, be specified for each experimental sample; where this has not been done, typical input parameters will be used instead.

B. DEPENDENCE ON CRYSTAL FACE

The purpose of this section is to consider the substantial effects of allowing variations in crystal face. This is accomplished by allowing variations about typical values of three parameters known to be structure-sensitive: ϕ_m, ϕ_f, and σ_f. These three are probably linked; that is, a certain substrate face (e.g., atomically flat 110) fixes ϕ_m, fixes the geometry and the density of adsorbate at a monolayer σ_f, and fixes the epitaxially grown work function of the monolayer film ϕ_f. But at the present there is no known correlation between them, so that their variations are arbitrarily presumed to be independent.

Figure 1 shows an analysis of these variations for the Cs-W system. Curve A is constructed with typical parameters using $\phi_m = 4.62$, $\phi_f = 1.81$, and $\sigma_f = 4.8 \times 10^{14}$. Curve B with ϕ_m arbitrarily increased by 10% lies slightly above A in the rising part of the S-curves. Curve C with σ_f arbitrarily increased by 10% rises slightly above B in most of the peak emission region. Curve D with ϕ_f arbitrarily decreased by 10% lies above curves A, B, and C. By combining the best characteristics – raising ϕ_m, lowering ϕ_f and raising σ_f each 10% – curve E is constructed.

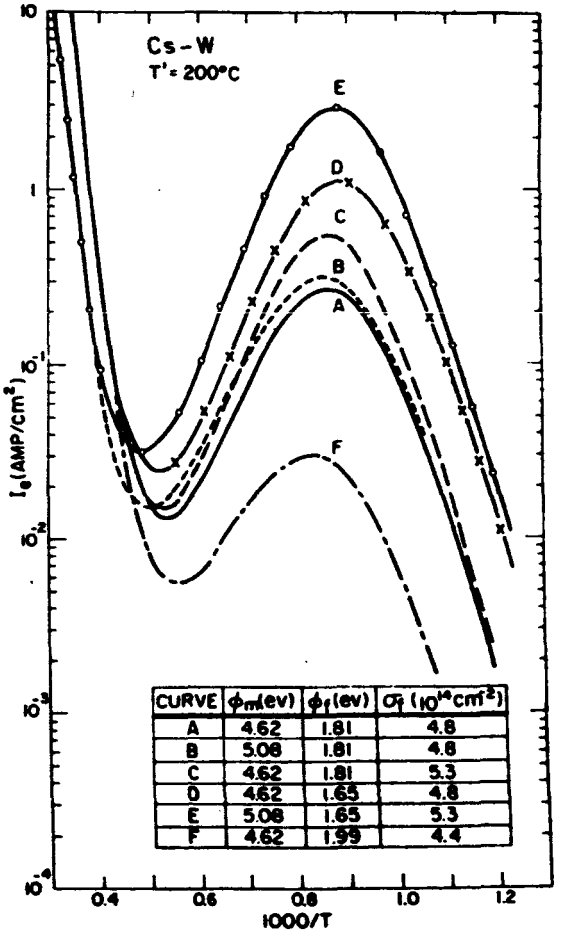

CURVE	ϕ_m(ev)	ϕ_f(ev)	σ_f (10^{14}cm^{-2})
A	4.62	1.81	4.8
B	5.08	1.81	4.8
C	4.62	1.81	5.3
D	4.62	1.65	4.8
E	5.08	1.65	5.3
F	4.62	1.99	4.4

Fig. 1. Theoretical plot of S-curves for Cs on different surfaces of W at T′ = 200°C. Input parameters which were allowed to vary in curves A-F are shown in the table.

Here the emission is an order of magnitude larger than the reference curve A. Curve F with a 10% decrease in σ_f and a 10% increase in ϕ_f lies about an order of magnitude below curve A.

The main conclusion to draw from this figure is: if for different crystal faces 10% independent variations in ϕ_m, ϕ_f, and σ_f are reasonable, then electron emission variations by an order of magnitude are reasonable. This theoretical conclusion is general in the sense that it should apply to many adsorbates and substrates. It has been qualitatively verified by many experimenters[8-10] and by quantitative thermionic experiments carried out in the presence of high electric field ($\sim 10^5$ v/cm) of Webster for Ta in Rb[11] and for Re in Cs.[12] But because of the possibility of unwanted background emission in Webster's experiments, his data for different crystal faces primarily have a relative, rather than an absolute, quantitative significance.

Another conclusion to be drawn from Fig. 1 is that some curves such as B and C cross over in the rising part of the S-curve region, while others do not. This conclusion is also experimentally verified.[9-12]

Finally, it must be noted that small percent variations in ϕ_f are much more effective in producing larger emission (and a lower work function) than independent similar percent variations in ϕ_m and σ_f. This conclusion cannot be checked experimentally at present. It does, however, seem to be in contrast to the current intuitive idea[5, 12] that the controlling crystal sensitive parameter is ϕ_m alone. But if the current idea were so, then *no* curves would cross in the rising part of the S-curves,[5] which is contrary to experiment. This current idea may be reconciled with the present study by presuming an appropriate coupling scheme between ϕ_m, ϕ_f, and σ_f.

C. S-CURVE DATA FOR Cs ON POLYCRYSTALLINE W, Mo, Ta, Nb, AND Re

In most of the data to follow the very important input parameters, ϕ_m, ϕ_f, and σ_f have not been specified by the experimenters. This omission of input information makes the comparison of theory with experiment less meaningful. There are two alternatives to take in comparing theory with such experiments: (a) use *typical* ϕ_m, ϕ_f and σ_f values (though they are not known to apply to the system of interest), or (b) use *adjusted* ϕ_m, ϕ_f and σ_f values to best fit the data. Both procedures are valid since these input parameters are in many cases not specified. But we choose alternative (a) in which one can theoretically construct S-curves without referring *back* to particular adsorption data. This agrees with the proposed policy of using no adjustable parameters in the equations. In particular, ϕ_f and σ_f are always taken for lack of other information as $\phi_f = 1.81$ ev characteristic of bulk cesium liquid and $\sigma_f = 4.8 \times 10^{14}$ cm^{-2} characteristic of the Taylor-Langmuir Cs-W system. Where ϕ_m is measured or measurable, it is always used; otherwise the typical value from Table 1 of ref. 2, is used.

Taylor and Langmuir[6] have empirically constructed a classic family of S-curves for Cs on W. Three of these ($T' = 237$°K, 270°K, and 313°K) are reproduced in Fig. 2 as the dashed lines.

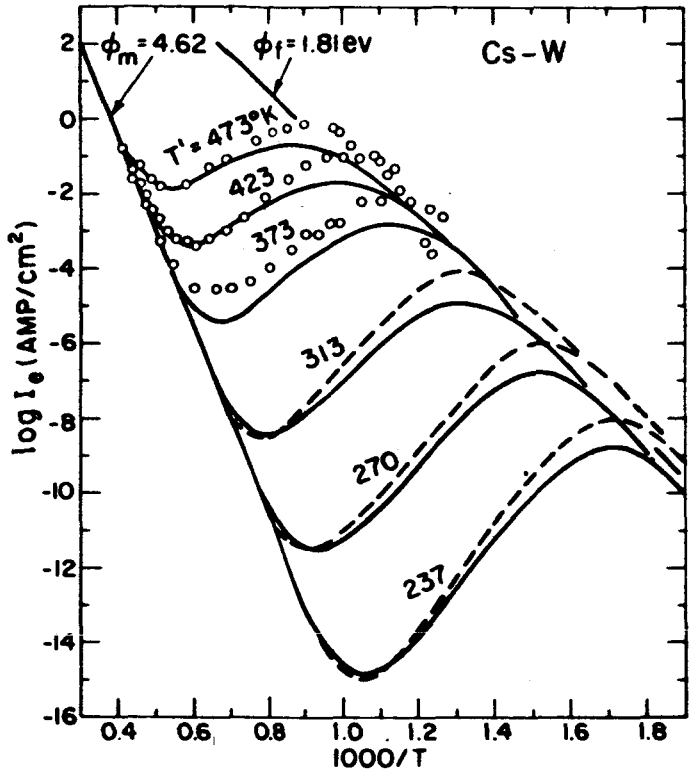

Fig. 2. Comparison of theoretical Cs-W S-curves (solid lines) with experimental data of Houston (dots) and of Taylor and Langmuir (dashed curves). T′ values of theory and experiment are identical.

They report ϕ_m = 4.62 ev, and $\sigma_f = 4.8 \times 10^{14}$ cm^{-2}. ϕ_f is observed to lie near 1.81 ev, but can easily be in error by ~ 3%. For comparison, a theoretical set of curves (4.62, 1.81, 4.8) are calculated at the same T′ values and are shown as solid lines in the same figure. Good agreement is evident over about nine orders of magnitude. The agreement would even be better if ϕ_f (which is not known accurately) were taken as 1.75 ev. Then a new theoretical set of curves (4.02, 1.75, 4.8) is calculated to more accurately pass through the data.

Houston[12] has measured S-curves for Cs on a different sample of W, but in a higher temperature range than Taylor and Langmuir. Typical values of his raw data taken at 473°K, and 373°K are shown as dots in the same Fig. 2. ϕ_m is seen to be 4.62 ev, in agreement with Taylor and Langmuir, but ϕ_f and σ_f are not specified. Nevertheless, for comparison, theoretical curves (4.62, 1.81, 4.8) are drawn as solid lines at the same temperatures. Good agreement is observed over 4 orders of magnitude (Houston reports that the high 373°K values are due to unwanted leakage). The agreement is calculated to be even better if other input parameters (4.62, 1.65, 4.5) are used instead.

Main conclusions from the Cs-W comparison of theory and experiment are: (a) It is possible to fairly accurately calculate electron emission over 14 orders of magnitude without using

adjustables and (b) the Taylor-Langmuir and the Houston polycrystalline surfaces, fairly accurately characterized by the parameters (4.62, 1.75, 4.8) and (4.62, 1.65, 4.5) respectively, show a close similarity.

Many S-curve data are also reported for the system of Cs on polycrystalline Mo. In Fig. 3 are shown raw data of Houston[12] and of Aamodt, Brown, and Michols.[13] ϕ_m seems to be 4.38 ev for both polycrystalline samples, but ϕ_f and σ_f are unknown. For comparison, a theoretical set of solid curves (4.38, 1.81, 3.8) is drawn on the same figure. Agreement is good over about 7 orders of magnitude. It would be better, of course, if the unknown quantities ϕ_f and σ_f were separately adjusted for each sample.

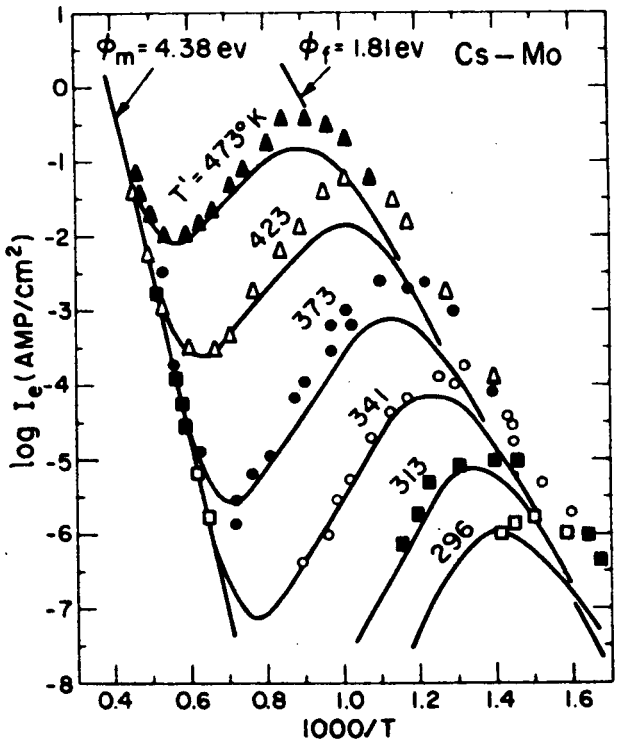

Fig. 3. Comparison of theoretical Cs-Mo S-curves (solid lines) with experimental data of Houston (▲, Δ) and of Aamodt, Brown, and Nichols (●, O, ■, □). T′ values of theory and experiment are identical.

S-curve raw data for Cs on Ta at T′ = 473°K taken by Houston[12] are shown in Fig. 4. ϕ_m, ϕ_f, or σ_f could not be determined. A typical theoretical curve A (4.19, 1.81, 4.8) is shown on the same plot for comparison and agreement is very good, except for the region to the right of the maximum. For further comparison, the "10% enhancement" curve B (4.61, 1.65, 5.3) and the "10% depressant" curve C (3.81, 1.99, 4.4) are also indicated. The data fall between these curves. It is estimated that the parameters (4.21, 1.65, 4.2) would more accurately fit the data.

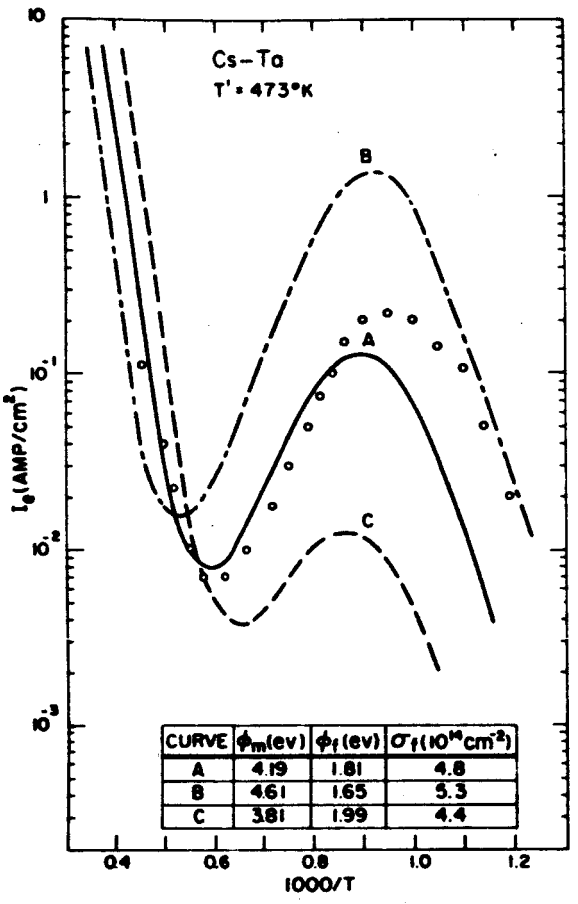

CURVE	ϕ_m(ev)	ϕ_f(ev)	σ_f(10^{14}cm^{-2})
A	4.19	1.81	4.8
B	4.61	1.65	5.3
C	3.81	1.99	4.4

Fig. 4. Comparison of three theoretical Cs-Ta S-curves (A, B, C) with experimental data of Houston (circles) at T′ = 473°K.

S-curve data for Cs on Nb at T′ = 473 have also been taken by Houston.[12] It is shown in Fig. 5 as circles. Also, (extrapolated) Cs-Nb data (T′ = 473) of Hatsopoulos and Kitrilakis[14] are shown in the same plot as squares. ϕ_m, ϕ_f or σ_f could not be determined. A typical theoretical curve A (4.01, 1.81, 4.8) is shown on the same plot; agreement is poor. For further comparison the 10% enhancement curve B (4.42, 1.65, 5.3) and the 10% depressant curve C (3.65, 1.99, 4.4) are also indicated. Agreement is still poor. It is estimated (from comparing Figs. 1 and 5) that an unusually low σ_f value, say $< 3 \times 10^{14}$, must be present for the Cs-Nb system, if theory and experiment are to match. Reasons for this are not clear since the lattice constants of Nb, W, Mo, and Ta are very similar.

Finally, S-curve data for Cs on Re have been reported by Houston,[12] but he suspected contamination, and also by de Steese,[15] but he found strong unexpected dependences on plasma properties, looking suspiciously like unwanted emission from emitter support, etc. An S-curve for Re with (5.10, 1.81, 4.8) is calculated to be very similar to W (4.62, 1.81, 4.8), shown as curve A in Fig. 1.

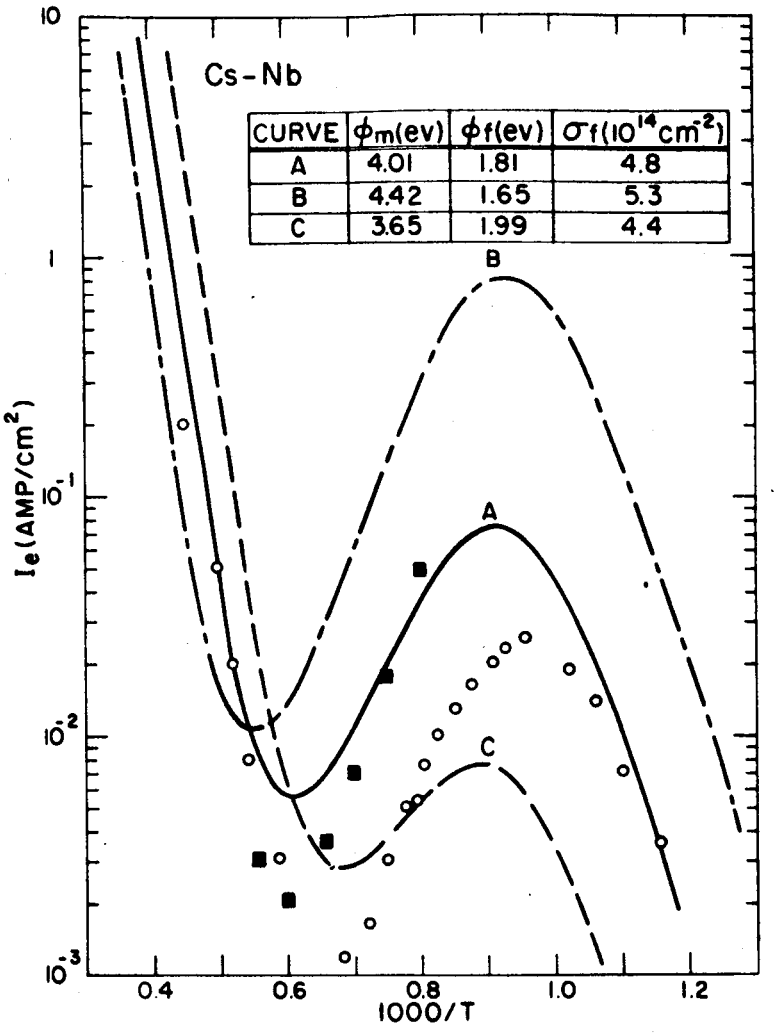

Fig. 5. Comparison of three theoretical Cs-Nb S-curves (A, B, C) with experimental data of Houston (circles) and Hatsopoulos and Kitrilakis (squares) at $T' = 473°K$.

There are many other studies on S-curves to be found in unpublished company reports and government reports. These curves give qualitative support to the previous theories but their quantitative value is questionable.

D. PREDICTION OF S-CURVES FOR Cs ON OTHER METALS

Because Cs is very important to thermionics, it may be significant to run a parametric study to evaluate S-curves for Cs on 21 transition metals. The S-curves are calculated at $T' = 200°C$ using typical parameters with ϕ_m from Table 1 of ref. 2, $\phi_f = 1.81$ and $\sigma_f = 4.8 \times 10^{14}$. The results are presented in Table I. For each element substrate, the emission minimum, emission maximum, minimum work function and the surface temperatures at which they occur are given.

TABLE I

CALCULATED S-CURVE PROPERTIES FOR Cs ON 21 TRANSITION METALS AT T′ = 200°C

METAL	EMISSION MIN.		EMISSION MAX.		ϕ_e MIN.	
	(amp/cm^2)	(1000/T)	(amp/cm^2)	(1000/T)	(ev)	(1000/T)
Ti	6×10^{-5}	0.74	5×10^{-4}	1.07	1.78	1.58
V	2×10^{-4}	0.69	1×10^{-3}	1.01	1.79	1.50
Cr	1×10^{-4}	0.63	6×10^{-4}	1.00	1.79	1.70
Mn	3×10^{-7}	0.96	5×10^{-7}	1.25	1.80	2.02
Fe	3×10^{-5}	0.75	1×10^{-4}	1.07	1.79	1.66
Co	4×10^{-5}	0.75	2×10^{-4}	1.07	1.79	1.64
Ni	1×10^{-4}	0.66	2×10^{-4}	1.01	1.79	1.78
Zr	1×10^{-3}	0.64	1×10^{-2}	1.00	1.76	1.29
Nb	5×10^{-3}	0.62	7×10^{-2}	0.93	1.78	1.18
Mo	8×10^{-3}	0.56	1.4×10^{-1}	0.88	1.78	1.23
Tc	7×10^{-3}	0.57	1.1×10^{-1}	0.89	1.78	1.24
Ru	4×10^{-3}	0.57	5×10^{-2}	0.91	1.78	1.27
Rh	2×10^{-3}	0.55	3×10^{-2}	0.93	1.78	1.32
Pd	4×10^{-5}	0.68	2×10^{-4}	1.05	1.77	1.68
Hf	5×10^{-3}	0.68	4×10^{-2}	0.94	1.78	1.22
Ta	8×10^{-3}	0.59	1.3×10^{-1}	0.90	1.78	1.15
W	1×10^{-2}	0.54	2.7×10^{-1}	0.85	1.77	1.19
Re	9×10^{-3}	0.50	1.5×10^{-1}	0.85	1.77	1.22
Os	2×10^{-3}	0.50	2×10^{-2}	0.95	1.78	1.46
Ir	2×10^{-3}	0.51	2×10^{-2}	0.92	1.77	1.35
Pt	4×10^{-3}	0.50	5×10^{-2}	0.90	1.77	1.30

The table shows that the emission from the first transition metal series – Ti, V, Cr, Mn, Fe, Co, and Ni – (and also Pd) is definitely an order of magnitude less than that of the other metals. This follows primarily because the *heats of sublimation* of the above metals is smaller, causing the partial covalent binding of Cs to be weaker ($\theta \sim 0.5$). In fact, Mn has the lowest heat of sublimation in the series and the correspondingly lowest emission.

Metals arranged in order of decreasing *minimum* emission are W, Re, Mo, Ta, Tc, Nb, Hf, Ru, Pt, Ir, Os, Rh, Zr, V, Ni, Cr, Ti, Co, Pd, Fe, and Mn. The metals arranged in order of decreasing *maximum* emission are W, Re, Mo, Ta, Tc, Nb, Ru, Pt, Hf, Rh, Ir, Os, Zr, V, Cr, Ti, Co, Ni, Pd, Fe and Mn. In general, the series of minimum emission and maximum emission are found to be very similar. It is significant to note that among the more highly emitting metals, W, Re, Mo, Ta and Nb, differences in crystal face qualitatively indicated in Fig. 1 can easily overshadow differences in the elements themselves.

Experimentally, Houston found,[12] for different metals in the same gaseous environment, that the order of decreasing maximum emission is W, Re, Mo, Ta and Nb in agreement with the

above predictions. Because of the great variety in possible crystal faces, the agreement is probably fortuitous.

It is also interesting to compare the above calculated series with a very approximate treatment[16] in which the simplified equation of state, $\phi_a(\theta) = \phi' T/T'$, is invoked. There it is found that, for comparable crystal faces, metals arranged in decreasing order of maximum electron emission are W, Re, Mo, Ta, Tc, Hf, Nb, Pt, Ru, Ir, Rh, Os, Zr, V, Ni, Cr, Pd, Ti, Fe, Co, and Mn. The parameter controlling this approximate series is ϕ_{ao}/ϕ_m where ϕ_{ao} is the calculated adsorption heat at $\theta = 0$. The comparison between this approximate series and the more accurate computer-calculated series shows very good agreement and adds partial justification for the simplifications made in the approximate treatment.

Finally, one should compare all the above series to the series of metals arranged in order of decreasing ϕ_m to show that ϕ_m is *not* the single important parameter as is currently supposed. That series is: Pt, Ir, Re, Ni, Pd, Rh, W, Cr, Rb, Os, Fe, Co, Tc, Mo, Zr, Ta, V, Nb, Ti, Mn and Hf. The general disagreement is evident.

Another result evident from Table I is that the minimum electron work function is fairly constant at ~ 1.78 for all 21 metals, even though ϕ_m values are very different. This result is not too surprising since in Fig. 1 it was shown that ϕ_f, not ϕ_m, is the more dominating influence in obtaining low work functions. Many experimenters have reported minimum work functions of the order of 1.4 ev, but it is the author's opinion that such values are characteristic of surfaces partially covered by an electronegative contaminant. It is well known, for example, that traces of oxygen[17] or fluorine[13] lower the minimum work function of Cs-coated emitters. The contamination effect in the system of Ba on W is just as striking. For example, Becker[18] early reported a pronounced work function minimum in the curve of ϕ_e versus θ. More recently, Moore and Allison[19] have shown that no such minimum (or a very shallow minimum) exists for clean Ba on clean W. Very recent and careful experiments[20] ($p \sim 10^{-10}$ torr) have definitely established that clean Ba on clean W gives no minimum whereas unclean Ba on clean W or clean Ba on unclean W gives a pronounced minimum.

In Table I approximate temperatures are given so that one can approximately reconstruct the 21 originally calculated S-curves, if desired.

It is possible, of course, to calculate S-curves for any combination of adsorbate, substrate and arrival rate without using adjustables. A general computer program has been set up for this purpose, which is available for loan to all workers interested in a parametric study of other systems, say, the other alkali metals on W. One main difficulty would be the establishment of typical σ_f values. Also, a main lack of incentive is the lack of experimental data for critical comparison.

E. CONCLUSIONS

The main general conclusion to be drawn from the study is that *no adjustable parameters* need to be used in fairly accurately predicting electron emission S-curves. They can be calculated for many metallic adsorbates, many metallic substrates, and over large temperature ranges.

Also, electron emission S-curves calculated for cesium on different substrates show that variations in crystal face, heat of sublimation, surface density at a monolayer, and other material properties are very important. The electron work function of the substrate is *not* the sole criterion for S-curve performance as others have intuitively suggested.

The study does not consider complications due to a patchy distribution of substrate properties. But this is not a drawback to the theory: if a patch distribution for a particular test surface is known *a priori* then the theory can be applied to each homogeneous patch separately. Besides, certain required input parameters such as the electron work function of the bare substrate imply an approximate averaging over existing patches.

II. A DIMENSIONLESS PARAMETER CHARACTERIZING ELECTRON EMISSION S-CURVES*

by
Jules D. Levine

A. INTRODUCTION

Immersing a pure metallic surface in a dissimilar metallic vapor greatly alters the electron emission. This effect is caused by the presence of an adsorbed layer partially covering the metallic surface. Conventionally, one displays this effect by plotting curves of log electron emission versus reciprocal surface temperature, at various constant values of arrival rate. These are called S-curves because of their characteristic shape. Typical families of S-curves are given by Taylor and Langmuir,[6] and by Houston and Webster.[12]

To analyze S-curve performance, Rasor[5] derived a correlation among (a) electron work function of a partially cesium-coated surface, (b) electron work function of the bare substrate metal, and (c) the ratio of the surface-to-bath temperatures. The correlation, together with the Richardson equation, yields S-curve performance, but the connection is not direct. In addition, the correlation must be of limited validity since it essentially represents a perturbation study of the reference Taylor-Langmuir Cs-W system; it cannot apply, for example, to other adsorbates such as Ba or Th. Other workers have not attempted to correlate or predict S-curves.

The purpose of this section is to give a simple approximate analysis of S-curves for different adsorbates, substrates, and arrival rates. The range of interest is the rising part $0.1 < \theta < 0.4$ of the S-curves where the equation of state is simple and where many cesium-coated thermionic emitters operate. This communication will be superseded later by more exact studies based on previously derived adsorption theories.[4]

B. THEORY

Consider a metallic surface at temperature T immersed in a vapor bath at temperature T′. A fraction θ of the surface is covered by the adsorbed particles. The relation between T, T′, and θ, obtained by rearranging the rate balance, is

$$\frac{\phi_a}{T} = \frac{\phi'}{T'} + \frac{1}{5050} \log_{10} \frac{\omega_a \nu \sigma_f \theta e \Delta S'/k}{\omega_a \nu' \sigma'} \qquad (1)$$

* Reported in Proceedings of Thermionic Specialists Conference, Gatlinburg, Tenn., IEEE October (1963).

where ϕ_a is the heat of adsorption (a function of θ), ϕ' is the heat of vaporization of the liquid, and all other terms are defined in reference 3. For the particular range $0.1 < \theta < 0.5$, direct calculation shows that the log term is negligible; then to a first approximation, the equation of state becomes (within an accuracy of about 7%)

$$\frac{\phi_a}{T} = \frac{\phi'}{T'} \tag{2}$$

This equation shows that the heat of adsorption, being a function of θ, is in turn a function of the ration T/T'. Rasor[5] was the first to recognize the importance of Eq. (2). He demonstrated that the electron work function, being essentially a function of θ, should also be a function of T/T' in the particular coverage range $0.1 < \theta < 0.5$ which corresponds approximately to the temperature range of about $2.5 < T/T' < 4.5$.

But one can proceed further and directly combine Eq. (2) with the Richardson equation, $\log (I/120T^2) = -5050\ \phi_e/T$, where ϕ_e is the electron work function of the partially coated surface, to obtain a simple, compact equation

$$\log \frac{I}{120T^2} = -\frac{5050\ \phi'}{T'} \cdot \frac{\phi_e}{\phi_a} \tag{3}$$

Now the dimensionless parameter ϕ_e / ϕ_a is a function of θ, but since ϕ_e and ϕ_a both fall linearly in the low θ region, the parameter can be crudely approximated by the particular parameter ϕ_{eo} / ϕ_{ao} evaluated at $\theta = 0$. If β is defined as $\beta \equiv \phi_{eo} / \phi_{ao}$, Eq. (3) approximately becomes

$$\log \frac{I}{120T^2} = -\frac{5050\ \phi'}{T'}\ \beta \tag{4}$$

which is the desired result. The two applications of this equation to relative S-curve performance will now be discussed.

C. APPLICATION TO FIXED ARRIVAL RATE

First consider the case where the arrival rate of vapor particles is fixed, which is essentially equivalent to having the quantity ϕ'/T' fixed. Then the ratio of electron emission for material combination 1 and 2 becomes

$$\log_{10} \frac{I_2}{I_1} = \frac{5050\ \phi'}{T'} (\beta_1 - \beta_2). \tag{5}$$

The visual interpretation of this equation is shown in Fig. 6. Note that materials with lower β should have greater emission. Typical calculated values[2] of β for cesium on different substrates on tungsten are given in Table II. For cesium on many different substrates it is seen that β is fairly constant. This result is not surprising since, qualitatively, those substrates having higher electron work functions ϕ_{eo} are also those having higher binding energies ϕ_{ao} for cesium. Subtle differences in β, however, can cause appreciable differences in electron emission. Thus, if $T' = 473°C$, $\phi' = 0.8$ ev, and $\beta_1 - \beta_2 = 0.03$, I_2/I_1 becomes equal to 4. Substrate-cesium combinations arranged in increasing order of β are W, Re, Mo, Ta, Tc, Hf, Nb, Pt, Ru, Ir, Rh, Os, Zr, V, Ni, Cr, Pd, Ti, Fe, Co, and Mn. This is in fair agreement with Houston's data[12] showing the S-curve performance to be in the order Re, W, Mo, Ta, Nb.

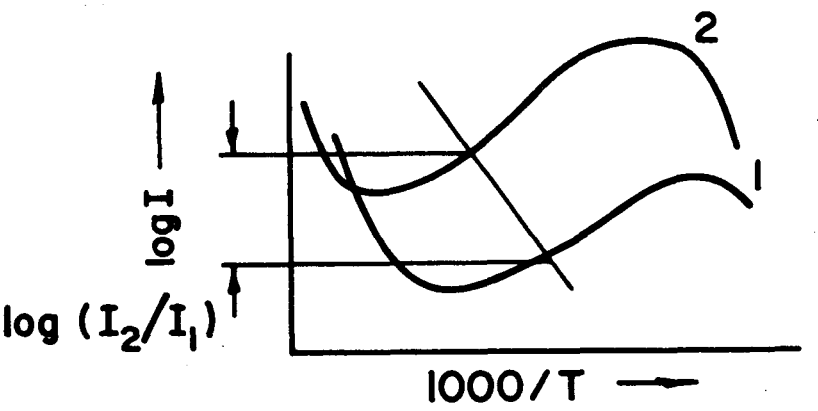

$$\log \frac{I_2}{I_1} = \frac{5050\phi'}{T'}(\beta_1 - \beta_2), \quad \beta = \frac{\phi_m}{\phi_{ao}}$$

Fig. 6. Arrival rate fixed (ϕ'/T' fixed). S-curves should have constant spacing equal to 10^{β} for fixed adsorbate, fixed substrate and comparable coverage.

Some adsorbate-tungsten combinations arranged in increasing order of β are Th, Mo, B, Al, Be, Ca, Ba, Lu, Sr, Mg, Na, K, Rb, and Cs. There are no S-curve data taken in a similar environment that are available for comparison with the above arrangement. One would predict, however, that for constant arrival rates, Cs and Rb are equivalent and Ba and Th are superior to Cs and Rb.

TABLE II

TYPICAL VALUES OF β FOR CESIUM ON DIFFERENT SUBSTRATES

SUBSTRATE	ATOMIC NUMBER	β	SUBSTRATE	ATOMIC NUMBER	β
Ti	22	1.92	Ru	44	1.67
V	23	1.95	Rh	45	1.70
Cr	24	1.86	Pd	46	1.71
Mn	25	2.24			
Fe	26	1.95	Hf	72	1.65
Co	27	1.95	Ta	73	1.62
Ni	28	1.85	W	74	1.60
			Re	75	1.61
Zr	40	1.77	Os	76	1.70
Nb	41	1.66	Ir	77	1.68
Mo	42	1.62	Pt	78	1.66
Tc	43	1.63			

TYPICAL VALUES OF β FOR DIFFERENT ADSORBATES ON TUNGSTEN

ADSORBATE	β	ADSORBATE	β
Cs	1.60	Ba	1.15
Rb	1.60	Sr	1.20
K	1.55	Ca	1.15
Na	1.38	Mg	1.34
Li	1.18	Be	.96
B	.62	Th	.58
Al	.90	Mo	.59

D. APPLICATION TO FIXED ADSORBATE AND SUBSTRATE

Next, consider the case where the adsorbate and substrate is fixed, which is essentially equivalent to having β fixed, but where the arrival rate E' is allowed to vary. Since E' is given by[1] $\log E' = A - 5050\,\phi'/T'$, Eq. (4) becomes

$$\log \frac{I_2}{I_1} = \beta \log (E_2'/E_1'). \tag{6}$$

The visual interpretation of this equation is shown in Fig. 7. In the customary case where the arrival rates differ by powers of 10, I increases by a factor 10^{β}, independent of T or T'. This simple prediction agrees with published Cs-W S-curves.[6, 12] For Cs on W, the predicted constant spacing is $\sim 10^{1.6}$ while the observed constant spacing is $\sim 10^{1.4}$, over many orders of magnitude.

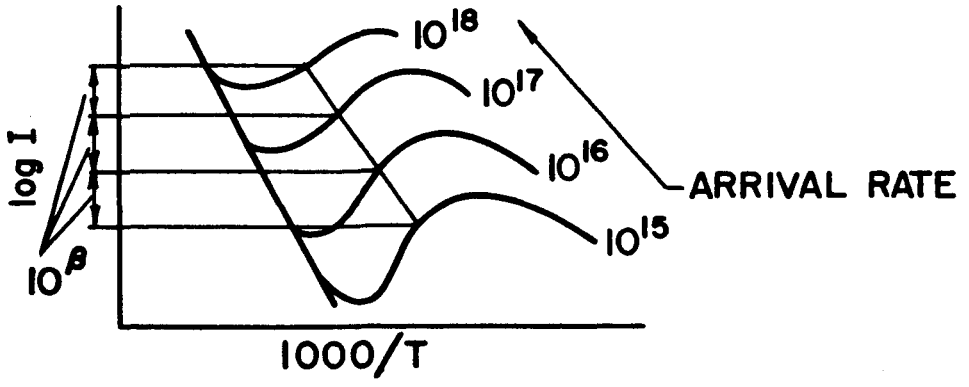

$$\log\left(\frac{I_2}{I_1}\right) = \log\left(\frac{A_2}{A_1}\right)^{\beta}$$

Fig. 7. Adsorbate and substrate fixed (β fixed). Materials with lower β should have higher electron emission for fixed arrival rate and comparable coverage.

E. CONCLUSIONS

A previously unrecognized dimensionless parameter $\beta = (\phi_{eo}/\phi_{ao})$ seems, in the first approximation, to control the relative performance of S-curves. The analysis is general in the sense that it does not rely on a particular model of the adsorption bond, and that it applies to many combinations of adsorbate, substrate, and arrival rate. It is significant that ϕ_{eo} does *not* appear to be the controlling parameter as other workers have intuitively suggested.

III. CESIUM ADSORPTION ON INSULATORS

by
Jules D. Levine

A. INTRODUCTION

The adsorption of a fractional monolayer of cesium on an insulator surface allows an electrically conducting path to be formed. From a practical point of view, a knowledge of the electrical conduction is important in designing thermionic converters. But the conduction is also a valuable and previously unrecognized diagnostic tool for determining the fraction θ of surface covered by adsorbed cesium, and other surface physics parameters.

Some interesting general features characterizing the cesium-insulator system are:

1. Cesium does not seem to spontaneously "wet" clean insulator surfaces. For example, glass tubes enclosing cesium at room temperature maintain relatively high resistances ($\sim 10^4\ \Omega$) for weeks without noticeable change.
2. The measured resistance is ohmic and reproducible over applied voltages of 0.1 V to 100 V and over a large range of temperatures. This indicates that electrons are *donated* to the host insulator conduction band and are *not* hopping from one cesium patch to another.
3. The conductance is proportional to the cesium pressure squared, at a given surface temperature.

Some experimental data for cesium adsorption on a glass surface are reported by Blackford.[21] He reports the general pressure squared dependence but his data are not very reliable since he mentions cesium attack on the glass. Also, he makes no attempt to interpret the data in terms of a theoretical model. Other workers[22, 23] have investigated conductivity of thin films (a few atom layers thick) of an alkali metal film deposited on an insulator surface, but they do not consider the fractional monolayer problem of interest in the present study.

A theoretical model based on observations (1), (2), and (3) above is presented below and is later compared with experiment.

B. THEORETICAL MODEL

Consider an insulator surface maintained at a temperature T immersed in a cesium vapor bath maintained at a lower temperature T′, as shown in Fig. 8. In steady state a certain fraction θ of the surface is covered with adsorbed cesium. The cesium is presumed fully ionized and presumed to donate its electron to the conduction band of the insulator. *Thus, a cesium film adsorbed*

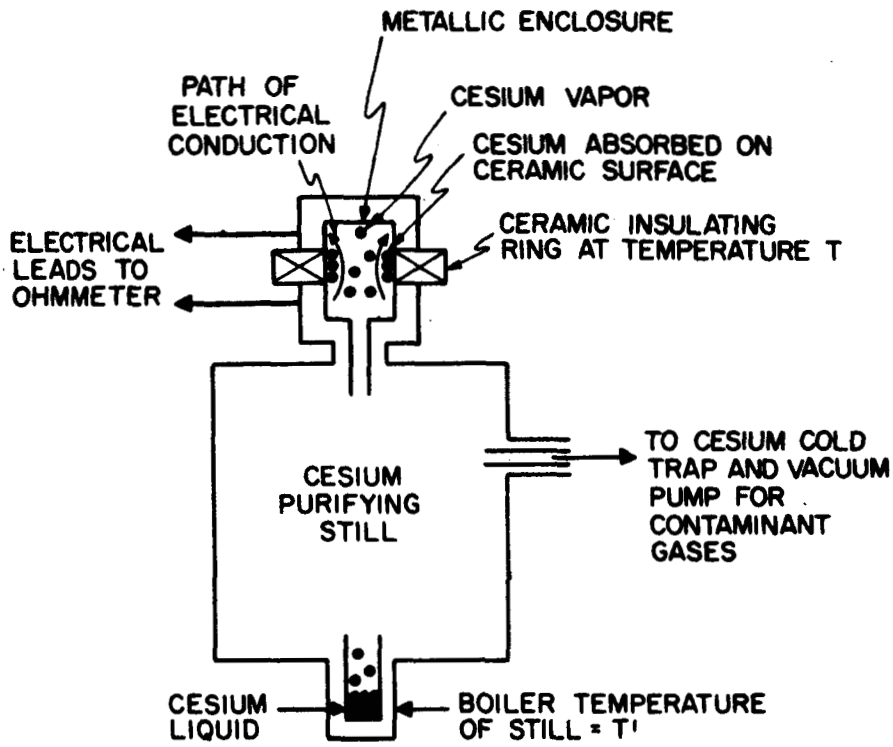

Fig. 8. Schematic experimental arrangement for measuring surface conductivity as a function of T and T'. The conductivity arises because adsorbed cesium donates an electron to the conduction band of the substrate ceramic insulator.

on an insulator acts as a semiconductor with an available and controllable amount of fully ionized donors.

One can monitor θ by simply measuring the surface resistivity $\rho_{\square}$ and using the standard relation

$$\rho_{\square} = (\sigma_f \, \theta \, q \, \mu)^{-1} \text{ (ohms)} \tag{7}$$

where σ_f is the cesium film density at a monolayer ($\sim 2 \times 10^{14}$ cm^{-2}),

q is the electronic charge (1.6×10^{-19} coulomb), and

μ is the electron mobility of the host ceramic, which will be calculated later.

Next one must determine the relationship of θ to T and T'. Because the conductance is proportional to pressure squared in the measured temperature range, one must conclude that the surface is more populated with ionized cesium diatomic molecules than with single cesium ions. Thus, θ represents the fraction of surfaces covered by diatomic molecules. Also, because the resistance lies in the range $10^3 < \rho_{\square} < 10^8$ one concludes that θ is a very small fraction of a monolayer. This important conclusion shows that the adsorbed species is very dilute. That is,

there are no complicating cesium-cesium lateral interactions on the surface. Simple adsorption physics should be used, and the heat of adsorption should be a true constant.

If it is presumed that a surface diatomic molecule vibrates about the center of mass with frequency ν, and is mobile like a two-dimensional dilute surface gas, then the chemical potential is:

$$\mu \text{ (surface molecule)} = kT \ln \left[\frac{\sigma_f \theta h^2}{4\pi mkT} \left(\frac{h\nu}{kT} \right)^2 \exp \left(-\phi_a / kT \right) \right] \tag{8}$$

Here h is Planck's constant
m is the mass of one cesium atom,
k is the Boltzmann's constant, and
ϕ_a is the adsorption heat referred to an arbitrary zero of a free cesium atom at infinity.

In equilibrium, the chemical potentials of all cesium species on the surface and in the vapor are stoichiometrically related. Thus, one can equate

$$\mu \text{ (surface molecule)} = 2\mu \text{ (vapor atom)} \tag{9}$$

where for an ideal vapor

$$\mu \text{ (vapor atom)} = kT \ln \left[\frac{N}{V} \frac{h^3}{2 (2\pi mkT)^{3/2}} \right] \tag{10}$$

In Eq. (10) the ratio (N/V) is the volume density of neutral vapor atoms. This volume density can be expressed in terms of the atom flux E′ through the vapor by the standard relation

$$E' = \frac{N}{V} \sqrt{\frac{kT}{2\pi m}} \tag{11}$$

E′ in turn is related to the vaporization rate of the cesium liquid bath by the theoretical equation derived in ref. 3:

$$E' = 2 \nu' \sigma' \exp \left(-\phi' / kT' \right) \tag{12}$$

where the factor 2 is the statistical weight of a vapor atom,
ν' is the liquid vibration frequency,
σ' is the liquid surface density,
ϕ' is the known vaporization heat, and
T′ is the vaporization temperature.

By combining Eqs. (8) to (12) the desired relation $\theta = \theta(T, T')$ is

$$\theta = \frac{(h\nu'\sigma')^2}{\pi\nu^2\sigma_f^3 mkT} \exp\left(\frac{-2\phi'}{kT'} + \frac{\phi_a}{kT}\right) \tag{13}$$

The above equation can be further simplified by presuming, for the lack of other information, that $\nu \sim \nu'$ and that σ' (of atoms) = $2\sigma_f$ (of molecules) = 5×10^{14} cm^{-2}. Then taking T as a typical value, say 400°K, Eq. (13) becomes

$$\theta = 1.1 \times 10^{-3} \exp\left(\frac{-2\phi'}{kT'} + \frac{\phi_a}{kT}\right) \tag{14}$$

Finally, by combining Eqs. (7) and (13) the desired theoretical resistivity relation is

$$\rho_\square = \frac{\pi\nu^2\sigma_f^2 mkT}{(h\nu'\sigma')^2 q\mu} \exp\left(\frac{2\phi'}{kT'} - \frac{\phi_a}{kT}\right) \tag{15}$$

or, if T is set equal to, say 400°K, $\rho_\square$ becomes

$$\rho_\square = \frac{2.4 \times 10^7}{\mu} \exp\left(\frac{2\phi'}{kT'} - \frac{\phi_a}{kT}\right) \tag{16}$$

Since ϕ' is known to be 0.747 ev, there are only two unknowns, ϕ_a and μ, to be determined in Eq. (16). By seeing if empirical resistivity data can be put in the theoretical form

$$\log \rho_\square = 7.38 - \log \mu + 7520/T' - 5050\ \phi_a/T \tag{17}$$

one could then calculate μ and ϕ_a and obtain a more comprehensive understanding of this adsorption system.

C. EXPERIMENTAL DATA

Experiments designed for proving the feasibility of Eq. (17) were conducted using an arrangement shown in Fig. 8. Details of the high vacuum apparatus and cesium still constructed by J. R. Fendley, Jr., are given in Section V. Metals, ceramics, and seals used were compatible with cesium in the measured temperature range 300°K < T, T' < 600°K. The purpose of the cesium still was to guarantee cesium purity.

Three preliminary tests made on cesium-glass systems showed that an unwanted trace contaminant appeared which increased the surface resistivity by as much as 4 orders of magnitude at room temperature. In the glass-cesium systems the undesirable contaminant (a) was bluish, (b) was more pronounced when kovar-sealing 7052 glass was used than when tungsten-sealing pyrex glass was used, (c) was most pronounced when hot liquid cesium interacted with

hot glass, and (d) was more volatile than cesium liquid. Glass-cesium tubes with a barium getter fired before tipoff showed a remarkable ability to purge the blue contaminant. In fact, the "blue" eventually migrated to the barium getter where it was probably most chemically stable. The room temperature resistances of many different glass-cesium tubes from previous experiments showed a remarkable similarity, indicating that there the contaminant is probably purged to a large extent. Room temperature ($T = T' = 300°K$) barium gettered tubes showed a resistivity $\rho_\square \sim 10^4\ \Omega$ per square, while tubes with no barium getter and a visible blue contaminant displayed resistivities in the range $10^6 < \rho_\square < 10^8$ ohms per square. High cesium purity is therefore essential in this very sensitive experiment.

Because of the purity problem the cesium-glass system was abandoned and a cesium-ceramic system continuously purified by a cesium still was investigated. The alumina ceramic used was thought to be Diamonite P-3142.

Special ovens were constructed to maintain T and T′ at separate and controllable values, because $\rho_\square$ was also very sensitive to temperature. In taking experimental data, $\rho_\square$ was measured as T was varied with T′ constant, and T′ was varied with T constant. A schematic representation of raw data is shown in Fig. 9. Here T, T′ and total resistance R are plotted versus time by a continuously operating Honeywell recorder. The temperatures are plotted using thermocouples and the resistivity is plotted directly from a Keithly 610 A ohmmeter connection. The constancy

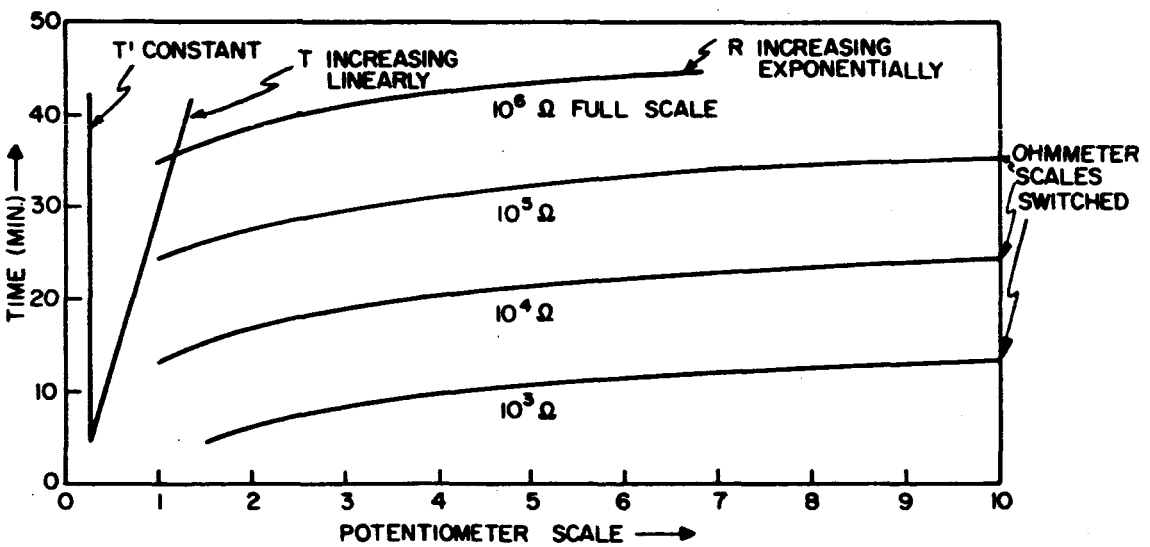

Fig. 9. Schematic raw data taken by a Honeywell recorder. T, T′ and R all are plotted vs. time.

of T and the logarithmic dependence of $\rho_\square$ on T′ are evident from this figure. This data and others taken in the same way are numerically analyzed and displayed in more useful forms in Figs. 10 and 11. Because of the ceramic ring geometry – I.D. = 1.915", width = 0.15" – the surface resistivity $\rho_\square$ was calculated from the measured total resistance R by the relation

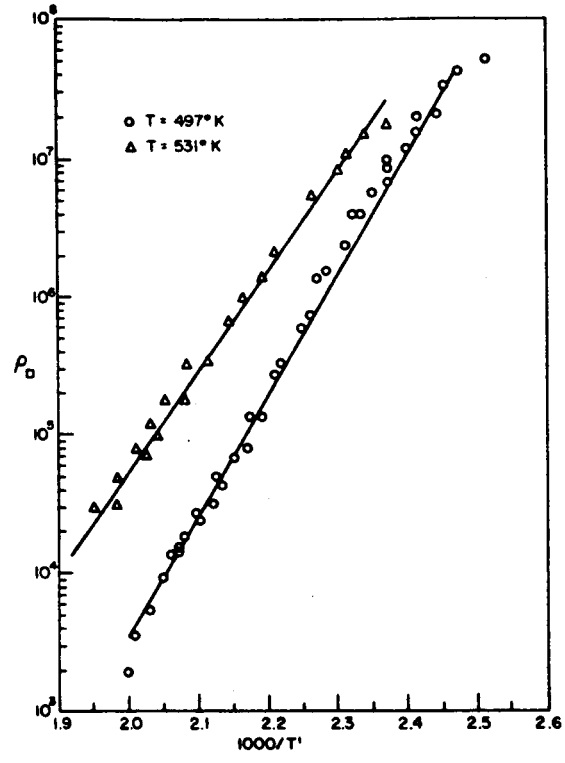

Fig. 10. Raw data of $\rho_\square$ vs. 1000/T′ at T = 497°K, and T = 531°K.

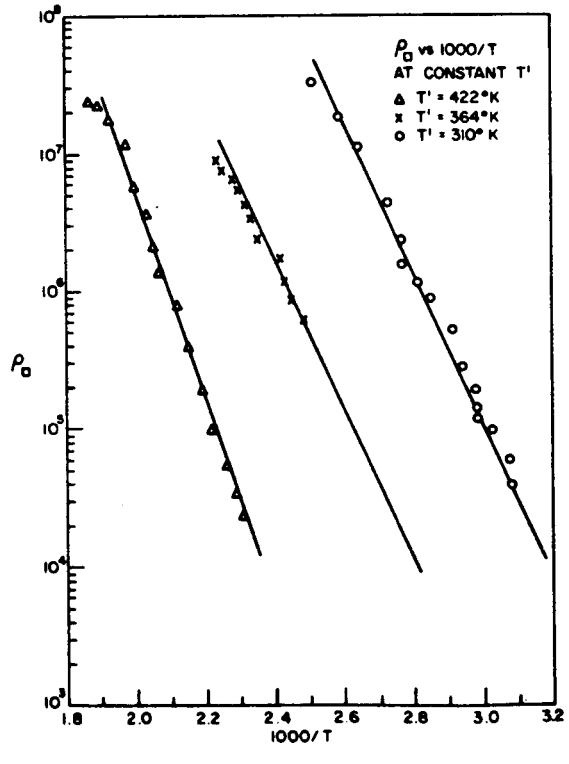

Fig. 11. Raw data of $\rho_\square$ vs. 1000/T′ at T′ = 422°K, T′ = 364°K, and T′ = 310°K.

$$\rho_{\square} = \frac{\pi \times 1.915R}{0.15} = 40R \tag{18}$$

The experimental results in Figs. 10 and 11 are essentially reproducible provided sufficient time is taken for quasi-equilibrium to be established in the heating and cooling cycles. The time constant depends strongly on T and is presently under investigation.

Finally the data in Fig. 10 and 11 (and other data which could not fit in these figures) are transposed and organized on a master graph shown in Fig. 12. Here points of constant $\rho_{\square} - 10^4$, 10^5, 10^6, and 10^7 ohms per square – are separately drawn as functions of reciprocal T and T′.

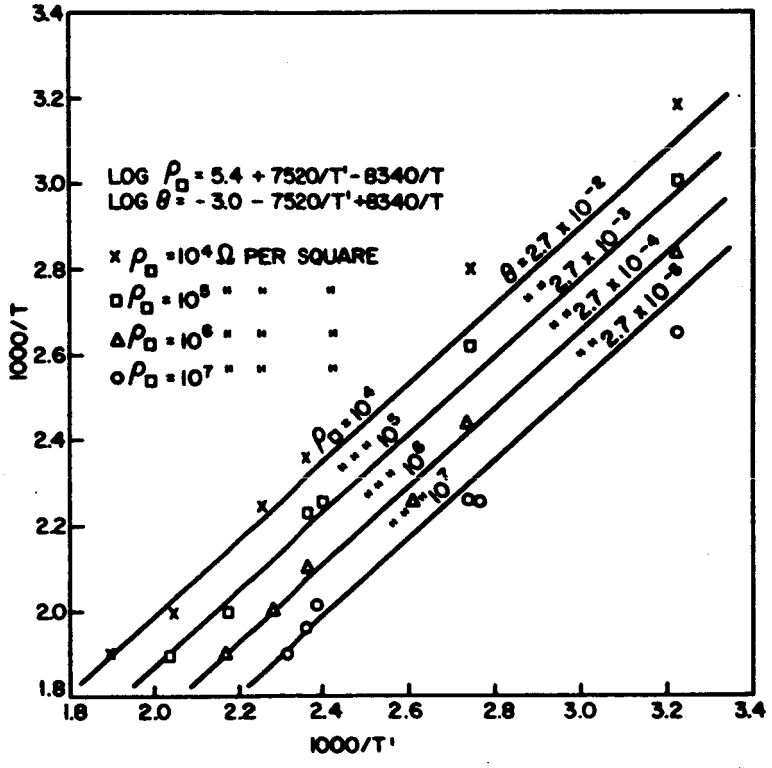

Fig. 12. Lines of constant $\rho_{\square}$ and θ for cesium on ceramic. According to theory, lines are parallel, equidistant and the horizontal line spacing is 0.13 units (corresponding to twice the heat of vaporization). The data agree fairly well with the line family.

An empirical analysis of the data in Fig. 12 shows that it can be represented as a family of straight parallel lines. In fact, the data easily fit the theoretical form of Eq. (17). Empirically,

$$\log \rho_{\square} = 5.4 + 7520/T' - 8340/T \tag{19}$$

By comparing Eqs. (19) and (20) one obtains

$$\phi_a = 1.65 \text{ ev}, \ \mu = 95 \text{ cm}^2/\text{volt sec} \tag{20}$$

ϕ_a is about twice ϕ' which is reasonable, and μ is of the order of the electron mobility in a CdS insulator which is also reasonable. Note that if molecular rotation on the surface were presumed then the partition function would increase by 10^4 and μ would be 0.01 $\text{cm}^2/\text{volt sec}$. This is unreasonable, so one concludes that there is no rotation. Finally, using $\phi_a = 1.65$, θ can be calculated from Eq. (14). It truly is much less than one monolayer as initially presumed in the derivation. The data and the theory seem compatible over the measured temperature range. Calculated lines of constant θ are also shown in Fig. 12.

The deviation of the points about the set of parallel lines may be due to experimental uncertainties. A more carefully designed experiment is presently being carried out, where the temperatures can be more accurately fixed and where the times to take the data will be longer to approach equilibrium more closely. It is expected theoretically that fine structure will emerge indicating the existence of single cesium ions.

But much is still unknown about the details of this system. Why are ionized molecules more copious than cesium ions on the surface? Are the molecules formed by surface diffusion or do they arrive directly from the vapor? What are the lifetimes and kinetics of the system? How is the work function altered by the cesium film?

There are at present no conclusive answers to these questions, but some preliminary studies have been made.

A calculation of the Hall effect shows that for this system the Hall angle α is given by

$$\alpha = \frac{10^{-8} \, C \, \mu \, H}{\pi \, L} \tag{21}$$

where C/L is the circumference to length ratio,
μ is the mobility ($\text{cm}^2/\text{volt sec}$), and
H is the magnetic field (gauss).

The equation is derived on the assumption that electrons are mobile but that adsorbed surface ions are not. A crude experiment to detect the effect showed a negative result, possibly indicating that the adsorbed ions are sufficiently mobile.

In other preliminary experiments, Xe was admitted to the adsorption cell. In all cases a noticeable and reproducible change of resistivity was immediately evident. But it was not clear whether the effect was due to the displacement of cesium molecules by Xe atoms on the surface, or to the unwanted effect of Xe on the operation of the cesium purifying still. (A slight variation in effective still temperature can be caused by the presence of sufficient Xe pressure.)

Addition of active pump gases and hydrogen showed unmistakable correlations with ceramic resistivity, but no quantitative data were obtained.

Finally, it was suggested by J. Fendley that since cesium does not wet the ceramic as much as a metal, it should be possible to measure thermionic emission from a metal in a closely spaced isothermal diode. A thin ring of ceramic insulator should be used to separate the metal electrodes, and the temperature should be adjusted so that thermionic emission is high while surface leakage is comparatively low. Preliminary tests by J. Fendley show that this idea is feasible and a special tube is being constructed for this purpose.

D. CONCLUSIONS

Theory and experimental data point to the following new model of cesium adsorption on an insulator surface.

The adsorbed cesium acts as a mobile two-dimensional surface gas. No patches exist, and the coverage is low, $\sim 10^{-4}$ monolayer. Because of lack of lateral interactions, the heat of adsorption is a constant, and its numerical value, referred to a free neutral atom, is 1.65 ev. Also, the cesium is adsorbed as a diatomic molecule which is singly ionized. The donated electron goes into the conduction band of the host insulator and the mobility of an electron in the host insulator is calculated from adsorption data to be 95 cm^2/volt sec. The total adsorption system resembles a semiconductor, but has the advantage of an easily variable and controllable population of ionized electron donors.

The experimental resistivity data is also helpful in determining temperatures of ceramic insulators to be used in thermionic energy converters. For this purpose an empirical equation and a master chart (Fig. 16) is included.

IV. ANALYSIS OF THE ARC MODE OPERATION OF THE CESIUM VAPOR THERMIONIC ENERGY CONVERTER*

by
K. G. Hernqvist

SUMMARY

An analysis was made of the cesium vapor arc discharge. It was assumed that the discharge operates in the ball-of-fire mode, that cumulative ionization via the two resonance excited states is the predominant ionization mechanism, and that trapping in the plasma of the resonance radiation results in a long effective lifetime of the excited states. A volt-ampere characteristic was derived for the cesium arc and the results were applied to the thermionic energy converter. Good qualitative agreement was obtained between theory and experiment.

* This material has been published in its entirety in Proc. IEEE 51, 748 (1963).

V. CONTINUOUS PUMPING OF CESIUM VAPOR DEVICES

by
J. R. Fendley, Jr.

A. INTRODUCTION

Certain devices, including thermionic energy converter tubes, depend for their operation on the presence of cesium vapor at a pressure of the order of one torr. The usual procedure for attaining this pressure is to seal off the evacuated device together with a cesium liquid reservoir. Cesium pressure in the device is then determined by the reservoir temperature, provided that the rest of the device is hotter. Impurity gases present in the cesium or evolving from parts of the device remain and may have harmful contaminating effects. An alternative to sealing off the device is to insert a cesium still between the device and a vacuum pump. In this way, a path may be provided for removal of gaseous contaminants, without an excessive loss of cesium.

B. CESIUM RECIRCULATION AND PURIFICATION

Cesium lost while pumping a vapor device may, with appropriate apparatus, be recirculated and purified in the process. A layout of apparatus for this purpose is shown in Fig. 13. Details of the cesium recirculation system or "still" are shown in Fig. 14. Several of the parts are commercial items, and the remainder is readily fabricated from stainless steel plate and tubing.

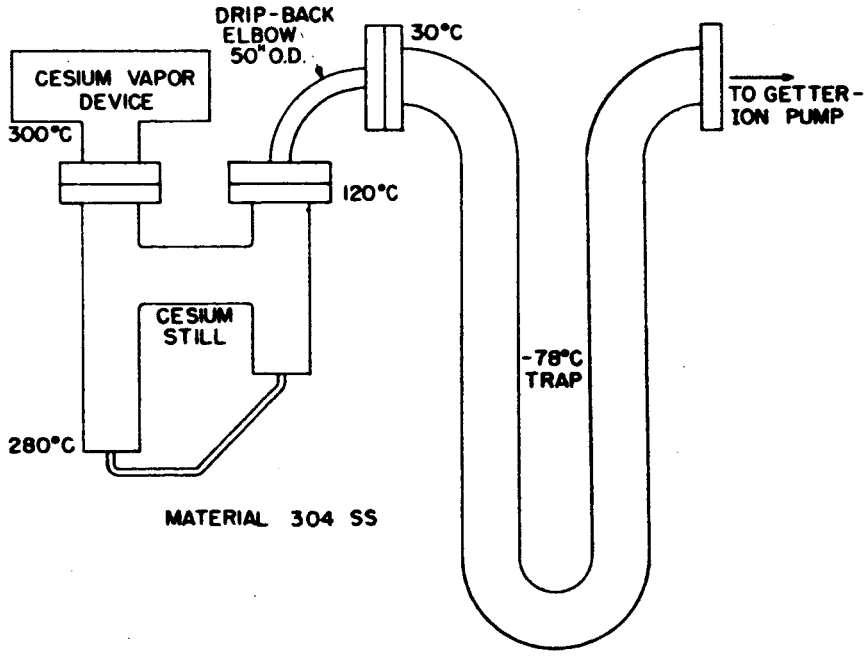

Fig. 13. Apparatus for continuous pumping.

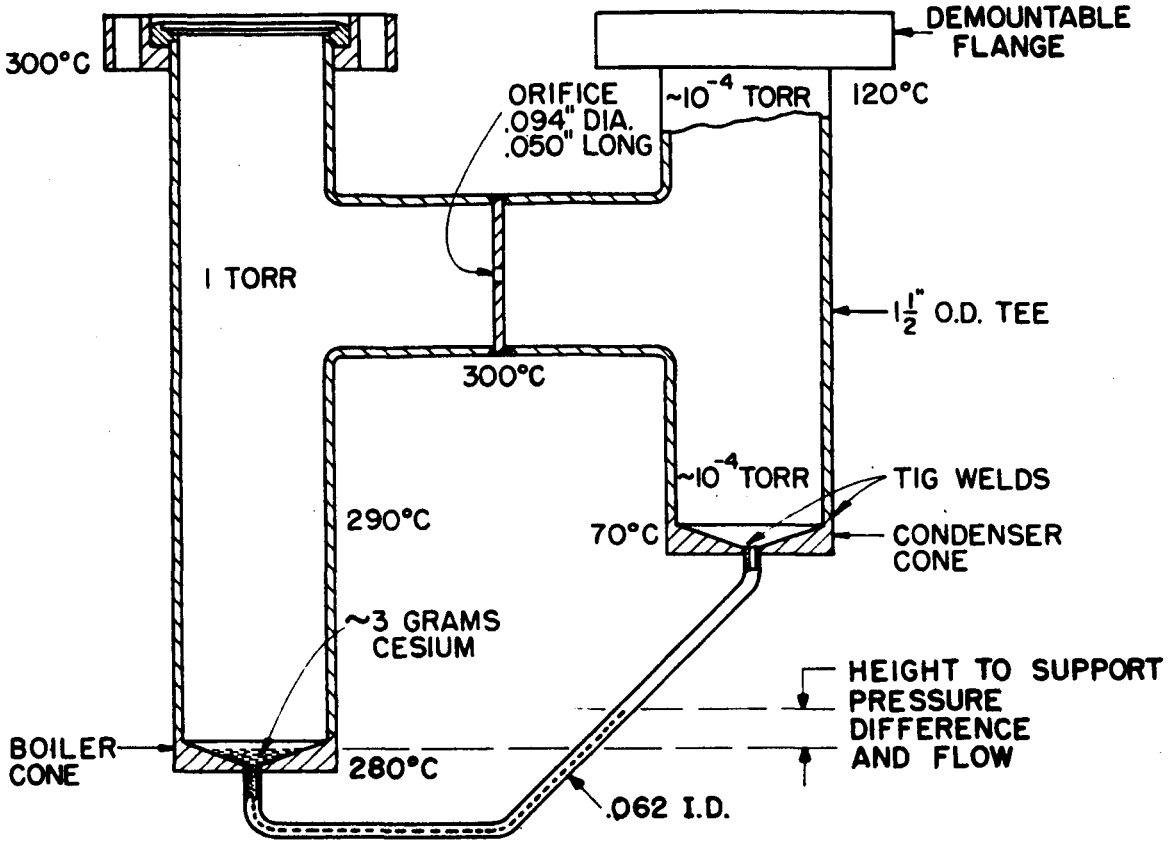

Fig. 14. Details of cesium still.

The boiler section and the condenser section of the still are connected by an orifice for vapor flow, and by a small tubing for liquid flow. The cesium liquid return scheme described here is similar to that described by Swartz and Napoli.[24] Typical temperature and pressure distributions are shown in Fig. 14. Cesium mass transport rates may be estimated from formulas in Dushman.[25] The conductance of the orifice is small (~ 1 liter/sec), compared to conductance from boiler to orifice (~ 100 liter/sec). Flow through the orifice therefore causes only a slight departure from thermal equilibrium in the hot side. The vapor pressure there is estimated to be within one percent of that which would be found in an equilibrium two-phase system with a cesium reservoir at the boiler cone temperature. Most of the cesium escaping from the orifice is condensed and flows back to the boiler cone through the 1/16" I.D. tubing. Some tiny fraction of this cesium rises to the top of the drip-back elbow and is lost to the dry ice trap.

Cesium may be initially introduced to the system from an appendage connected to a tee or cross on either the boiler or the condenser side of the still. Introduction of cesium on the boiler side has been found to be more satisfactory, because addition of plumbing on the condenser side introduces re-entrant pockets which may act as cesium sinks and prevent the proper gravity return flow.

C. REMOVAL OF IMPURITY GASES

Impurity gases may flow through the orifice, past the condenser section and cold trap, to be finally collected in a getter-ion pump or other suitable vacuum pump. Some active gases react with cesium and form compounds in the colder regions of the still or trap. Several pumping mechanisms therefore contribute to reduce impurity gas level below that which would obtain in a system without a region which is colder than the cesium liquid reservoir.

Mass spectrometer analysis of the outgassing from an operating cesium diode revealed that hydrogen was the principal impurity gas passing the cold trap. Removal of hydrogen by distillation is a slow process, and it has been found that a palladium membrane connected to the boiler side of the apparatus is more satisfactory for this purpose. One simply exposes palladium to high pressure hydrogen-contaminated cesium on one side, and to air on the other side. A thimble demountable flange construction suitable for this purpose is shown in Fig. 15. The thimble is heated by conduction from the flange to about 300°C, and hydrogen pumping takes place when an oxidizing atmosphere is present inside the thimble.

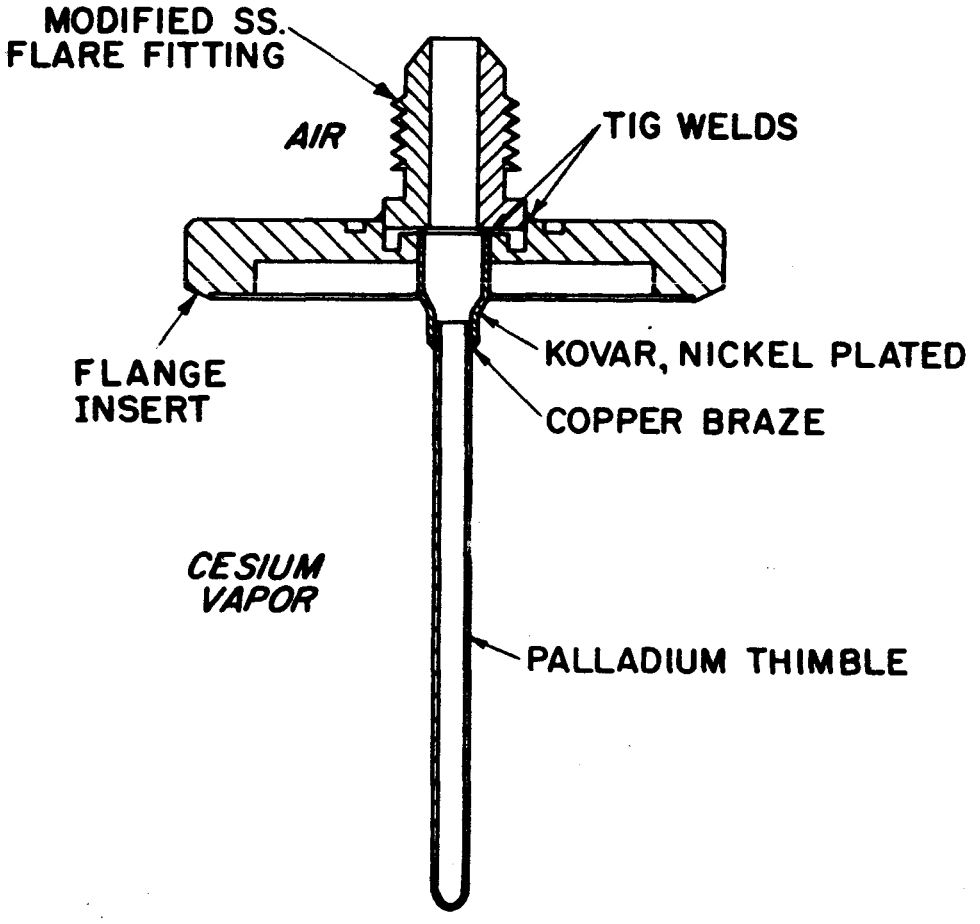

Fig. 15. Hydrogen port.

D. PURPOSEFUL GAS INTRODUCTION

The same palladium thimble may be used for experiments in which hydrogen introduction is desired. The oxidizing atmosphere (air) inside the thimble is in this case replaced by hydrogen. It should be mentioned, however, that a sudden change from hydrogen to air while the palladium is hot causes catastrophic heating and destruction of the palladium tubing. Recent results on hydrogen pumping with palladium have been reported by Young.[26]

The cesium still and trap combination has also been used in a system for investigating the effects of inert gases on a cesium vapor diode. Inert gas inlet valves, pressure gages and pumps need not be compatible with cesium vapor when a cold trap separates such components from the cesium section of the system.

E. SUMMARY

It has been found feasible to pump continuously cesium vapor devices operating at pressures of the order of one torr. Thus, a low contamination level may be achieved, which improves with time. Known impurity gases may be introduced whenever such gases are desired.

F. ACKNOWLEDGMENTS

Thanks are due Dr. K. G. Hernqvist for many helpful discussions. D. C. Pultorak and H. K. Freitag gave valuable assistance in construction of the apparatus.

VI. GAS ANALYSIS STUDIES

by
J. R. Fendley, Jr.

Apparatus for continuous pumping of a cesium vapor device is described in Section V. Such apparatus has been used with several cesium diodes in a system which included a mass spectrometer for gas analysis. The usual system is shown schematically in Fig. 17. It is important to note that the mass spectrometer analyzes only the gas present in the high vacuum mainfold of the system, which is pumped by the getter-ion pump. It is difficult to relate pressure in this manifold to partial pressure in the cesium section. Nevertheless, some interesting analysis findings were made, which give helpful guides to system design and operating procedure. A list of gas analysis findings is given below.

A. MASS SPECTROMETER USED AS LEAK DETECTOR

The mass spectrometer is useful and important as a leak detector. Several incidents occurred involving leaks which limited ultimate pressure to $\sim 10^{-7}$ torr. These leaks were readily pinpointed and corrected. Several other leaks limited system pressure to about 3×10^{-9} torr with the 8 liters/second pump in use. Such leaks, caused by porous stainless steel in some of the demountable flanges, probably would never have been found if the mass spectrometer had not been included in the system. These small leaks ($\sim 10^{12}$ molecules/sec) are a real plague, in that they escape detection in a routine component leak check and show up only after bakeout. Yet such leaks may be of great significance in fractional monolayer surface physics.

B. HYDROGEN, THE PRINCIPAL IMPURITY GAS

Hydrogen was the principal impurity gas observed during diode operation. It was found that most of this hydrogen originated in the cesium supply. Some 100 micron-liters of H_2 per gram of cesium was observed during a typical 10-hour initial operation. The palladium thimble device shown in Fig. 15 was constructed to speed up the removal of hydrogen. It appeared that this thimble was ten times or so faster than distillation for the removal of hydrogen. That is, with the thimble, hydrogen pressure of 10^{-8} torr was observed at a time when $\sim 10^{-7}$ torr would be expected from experience without the thimble. (There was no evidence either that hydrogen concentration was significant in cesium diode operation.)

C. PUMPING WITH CESIUM STILL – COLD TRAP ARRANGEMENT

CO and CO_2 are effectively pumped by the cesium still – cold trap arrangement. Before introduction of cesium, the emitter and other system parts were raised to their normal operating

temperatures. A pressure of CO of 10^{-7} torr was typical. Upon introduction of cesium, this would drop to $\sim 10^{-9}$ torr. Since evolution of CO likely continued at the same rate, it was concluded that cesium in the still and trap getters most of the CO evolved during normal operation. Similar results were observed for CO_2.

D. XENON INDIGESTION

Simple getter – ion pumps are not satisfactory for pumping xenon. This is evidenced by the mass spectrum shown in Fig. 16. Except for the presence of xenon, this spectrum is typical of that observed after a few hours of cesium diode operation. The xenon (easily identified by the natural isotope distribution) was left over in the getter ion pump from a previous xenon-dosing

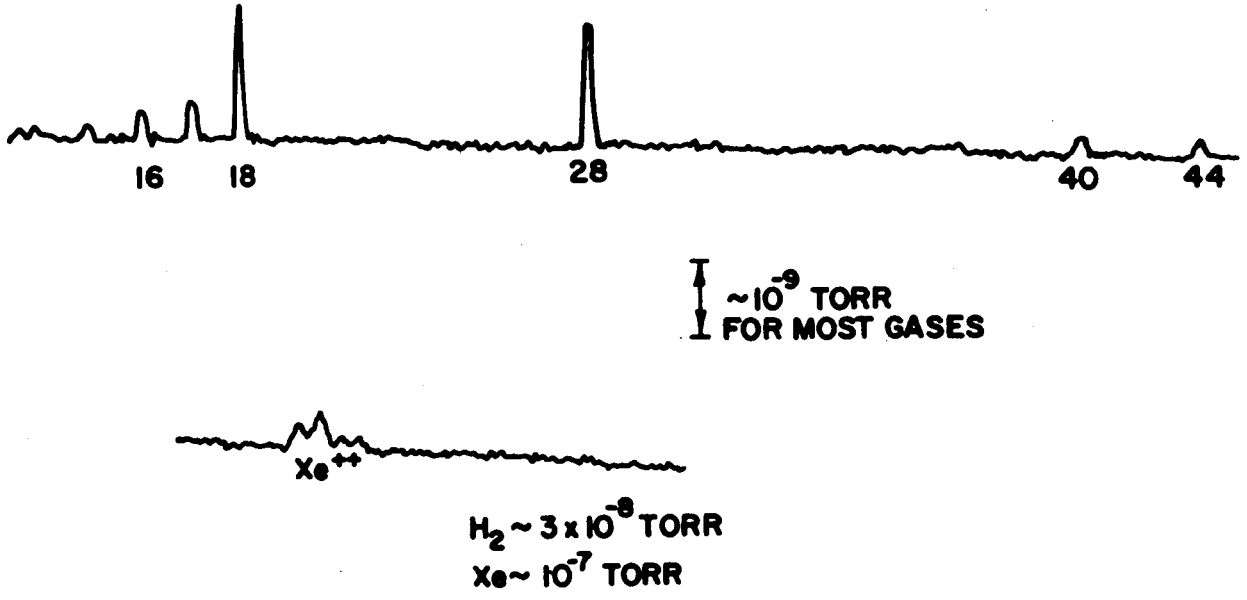

Fig. 16. Mass spectrum after a few hours of diode operation; cesium temperature 220°C.

experiment. Some xenon remained even after the pump was baked at 400°C. Xenon pumping is not stable; that is, xenon is alternately pumped and evolved in a complicated pattern influenced by the pumping of other gases. Such behavior with inert gas is well known.[27] The particular getter – ion pump used (Varian Model 911-5000) had been greatly overloaded by pumping some 30 micron-liters of xenon gas.

VII. DOSING OF THERMIONIC CONVERTERS WITH NOBLE GASES

by

J. R. Fendley, Jr., and K. G. Hernqvist

A. INTRODUCTION

Cesium diode thermionic energy converter tubes are being developed for the direct conversion of nuclear, chemical or solar heat to electricity. Only the solar heat source is "clean"; heat from the other sources is accompanied by fission or combustion products. Even in the solar tube case, there is the possibility of contamination due to outgassing from tube materials and reactions of cesium with these materials. The general problem of contamination is quite complicated, since it involves chemical reactions in a cesium liquid reservoir, and fractional monolayer surface effects, as well as volume collision effects. Inert gas experimentation was decided upon in order to minimize these complications. First experiments were performed with xenon and krypton, which are fission product gases to be found in nuclear reactors.

B. GAS DOSING SYSTEM

The system for introducing xenon and krypton is shown schematically in Fig. 17. It consists of a cesium section and a vacuum section, separated by a cold trap. Details of the cesium still are described in Section V.

Components in the vacuum section are never exposed to cesium vapor and need not be compatible with cesium. An inert gas supply and gas inlet valve are connected to the vacuum section. Typical operating procedure is as follows: All components except the mechanical pump and its trap are baked at 400°C while pumped by a conventional mercury vapor diffusion pump system. Then the system is sealed off and the getter ion pump is operated. A copper capsule containing about 3 grams of cesium is opened, and the arc mode diode is operated for some hours until operation appears stable. During this time, residual gas pressure drops, and it is usually found that the tube improves slightly, gaining perhaps 50 mv output voltage and then leveling off in performance. The improvement seems to be associated with heating of the collector to about 700°C. A degradation in performance with time (slumping) noticed on earlier experimental tubes has not been noted with the tube reported here. The improvement may be due to use of high purity nickel (Inco 270) for the collector. Recent experience with continuous pumping has been that performance slowly improves, and after perhaps 50 hours operation, the tube seems quite stable. The experimental tube is shown in Fig. 18.

Whenever inert gas introduction is desired, the getter ion pump power supply is turned off and the gas inlet is opened until the Pirani gage reads the desired pressure. The mechanical pump

is used to remove inert gas and restore the system to cesium only operation. The molecular sieve-type foreline trap minimizes the back diffusion of oil and water vapor from the mechanical pump.

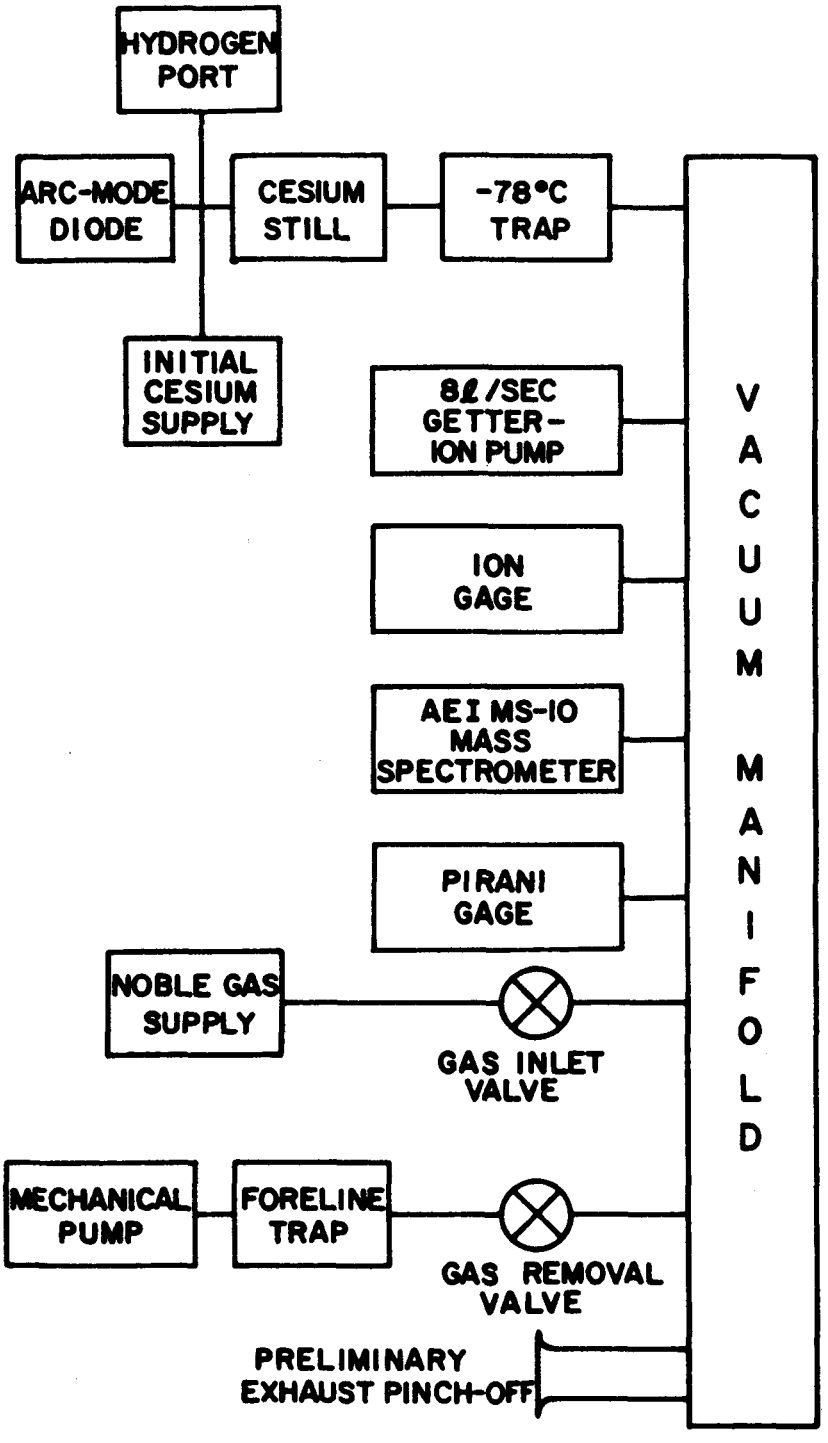

Fig. 17. System for gas analysis and gas dosing.

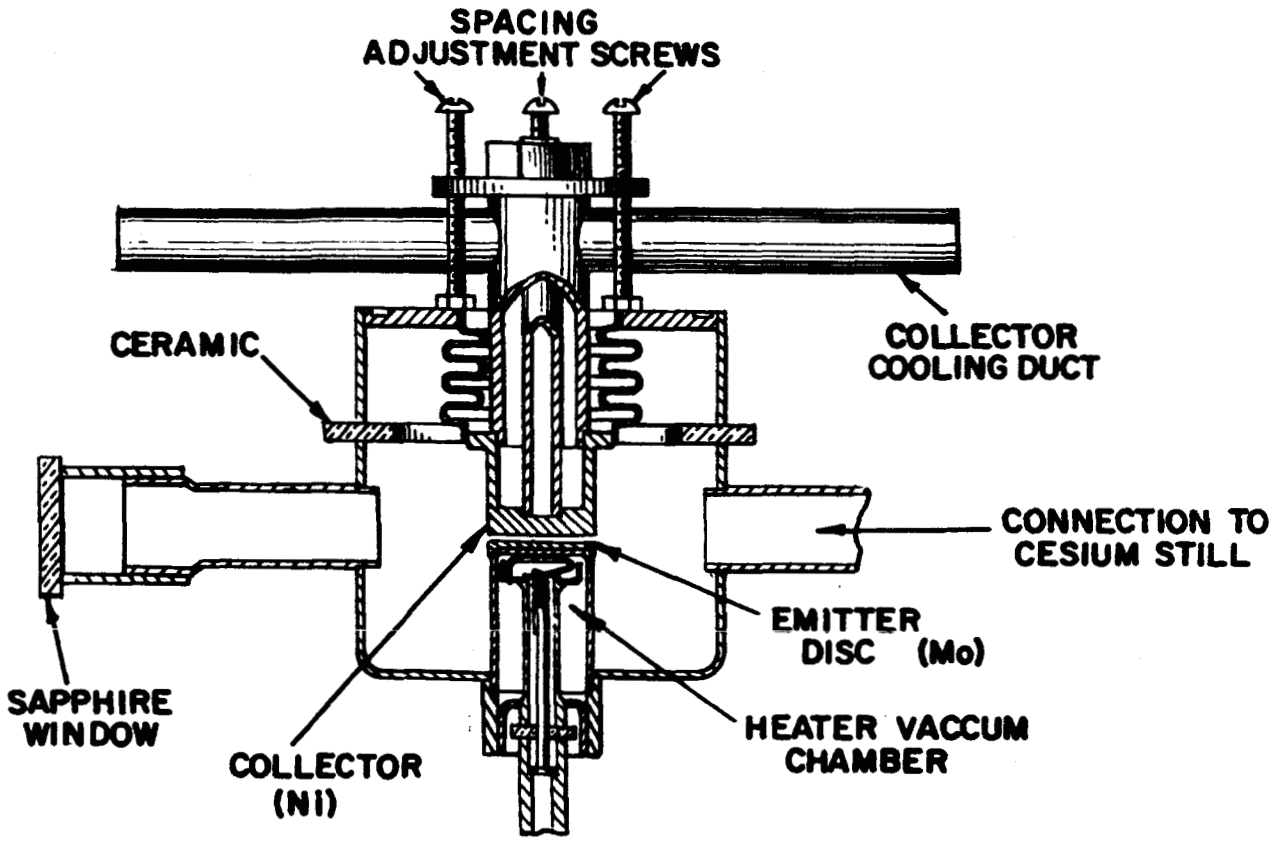

Fig. 18. Adjustable spacing arc-mode cesium diode.

C. EXPERIMENTAL RESULTS

Data on xenon dosing effects are shown in Fig. 19. The 2-torr curve is nearly the same as is obtained with no inert gas present. Even at 50 torr the effect is small. The effect of spacing variation is shown in Fig. 20. Figure 21 includes tracings of spectra taken during DC operation of the tube with and without xenon. An obvious effect of xenon is the broadening of the 0.852 μ and 0.894 μ resonance lines. The broadened spectrum resembles that reported by Thomas and Herman[27] and attributed by them to existence of CsXe molecules.

Effect of krypton introduction is shown in Fig. 22. Results are about the same as for xenon.

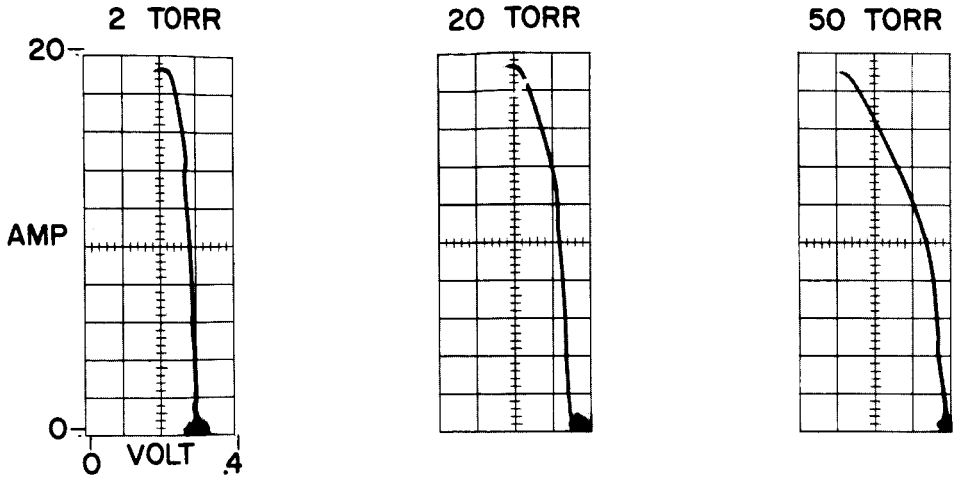

Fig. 19. Effect of xenon.

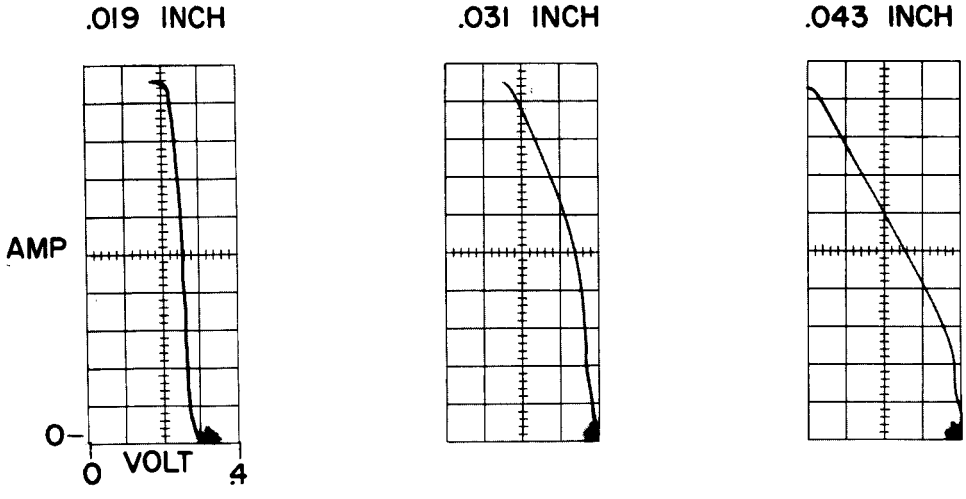

Fig. 20. Effect of spacing.

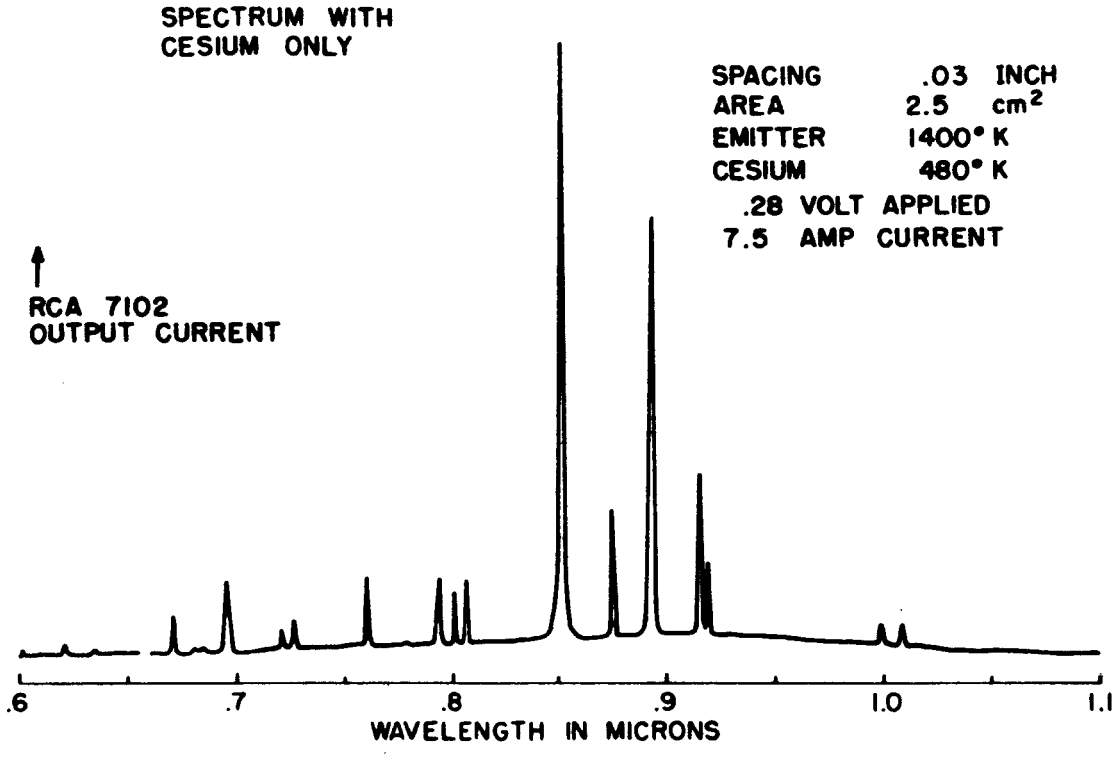

(a)

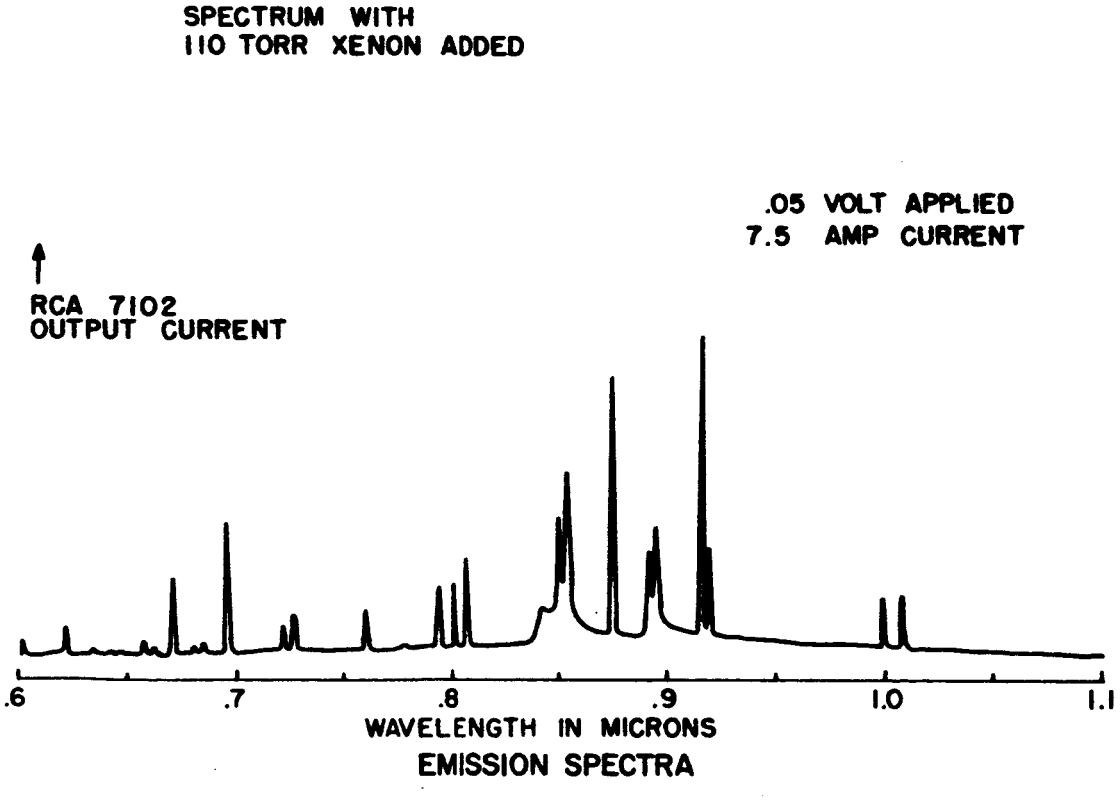

(b)

Fig. 21. Tracings of spectra taken during DC operation of the tube with and without xenon.

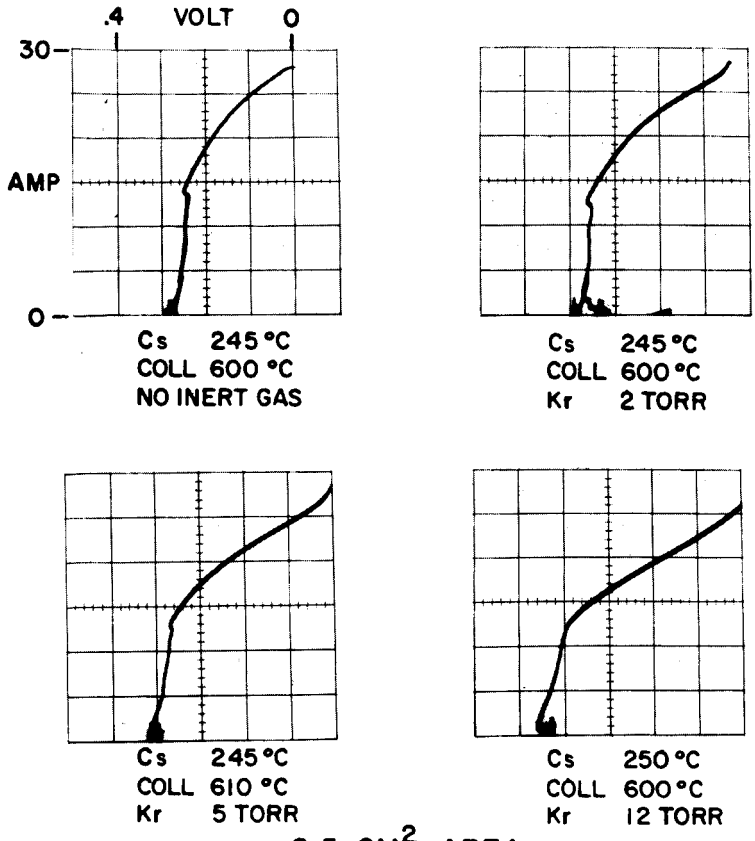

Fig. 22. Effect of krypton introduction.

D. DISCUSSION OF RESULTS

The gas dosing studies described here were performed on thermionic converters operating in the arc discharge mode. As seen in the illustrations the effects of noble gases at pressures up to several tens of torr on the electrical performance of the converter are observable but generally of a second order. From an experimental point of view the introduction of noble gases at these pressures introduces a flow impedance between the cesium pool and the diode space. Changes in the pool temperature do not exert themselves in a immediate change of cesium pressure in the diode space. Times of the order of an hour are required to reach new equilibrium. Since the cesium pool used in these experiments involves a cesium flow cycle, a certain experimental error in the cesium pressure at the diode space results due to the gas dosing.

The experimental results may be summarized as follows. Three changes in the volt-ampere characteristic are observable due to noble gas dosing. (1) The characteristic becomes smoother, exhibiting less of the sharp kinks and bends present for the pure cesium case. (2) There is a shift toward higher output voltage at low currents. (3) There is less output voltage available at higher current levels. Visual observations indicate that the glow region in the interelectrode space becomes more uniformly distributed covering the whole cathode area at all current levels. The cesium emission spectrum shows no large changes due to gas dosing.

Noble gases can theoretically affect surface properties, plasma generation rate, or plasma transport properties of the converter. Anode surface effects are possibly observable at the highest gas pressures used. They could be a factor contributing to the increased output voltage at low currents by lowering the anode work function. Lowering of surface work functions due to adsorption of noble gases has been experimentally observed.[28]

Visual inspection of the plasma glow region in an operating thermionic energy converter shows that for the pure cesium operation the glow often occurs as one or more isolated regions separated by dark plasma. This is a well-known phenomenon observed for the ball-of-fire mode of discharge in noble gases.[29] The glow plasma, which is the center of ionization, is separated from the cathode by a dark plasma. Most of the electron transport occurs from the cathode only at points facing a glow plasma, leaving part of the diode useless. The actual emission current density therefore varies along the cathode surface. These regions of glow sometimes jump back and forth between different positions resulting in sharp kinks in the volt-ampere characteristic. The position and shape of these glow regions is determined in a complicated manner by the boundary conditions that must be met to assure a Langmuir double sheath between dark plasma and glow plasma. These boundary conditions can be affected by magnetic fields.[29] Gas dosing of a cesium diode with noble gases results in a glow region which is uniformly distributed throughout the diode space. The corresponding effects on the electrical behavior are twofold. First, they result in a volt-ampere characteristic more free from sharp kinks and bends. Secondly, at current below saturated current the actual current density becomes lower since the current density becomes uniform along the cathode surface. This results in a larger effective work function (ϕ_{eff}) and a larger output voltage. This effect then is another possible contribution to the observed increase in output voltage as a result of noble gas dosing.

Perhaps the most pronounced effect of gas dosing is the reduction in output voltage at high current levels. Studies of electron emission of cesium-covered molybdenum[13] show that for the conditions corresponding to Figures 19, 20, and 22 the saturated emission current density is less than 3 amperes. It is believed that the part of the current above this limit is drawn from the supporting heat dam of the cathode. The transport properties of the plasma outside the diode space are not well understood but apparently strongly affected by gas dosing as well as interelectrode spacing (Fig. 20).

E. CONCLUSIONS

Noble gas dosing of thermionic converters has little effect on the electrical performance of the converter at pressures up to several tens of torr. Several fringe effects of gas dosing are expected which make noble gas dosing a desirable feature for thermionic converters: (1) Improved stability of electrical characteristics. (2) The discharge becomes more uniform, eliminating effects of surface inhomogeneities. (3) Greater ease of discharge ignition. (4) Less material transport from cathode to anode which results in increased life of converter. (5) The tube becomes more sluggish in its reaction to cesium bath temperature changes. This will tend to eliminate transients in large systems. (6) It offers promise for utilization of reactor fluxes (e.g., gamma radiation) for assisting ionization of the gas. This effect is discussed further in Section VIII.

VIII. EVALUATION OF THE POSSIBLE USE OF REACTOR RADIATION AS ADDITIONAL IONIZATION MECHANISM IN THERMIONIC DIODES

by
H. Hendel

A. INTRODUCTION

Recently, it was established experimentally that Xe at a pressure of 250 torr can be added to the cesium-plasma thermionic diode without significant deterioration of the efficiency. An evaluation of the possible use of the reactor radiation as an additional ionization mechanism has been performed. This additional ionization could conceivably allow operation either at lower temperatures or at higher output voltages for a given cathode temperature. Maintaining the basic Cs pressure to determine the work functions circumvents the difficulties plaguing rare gas (only!) converters due to the necessity of maintaining a low anode work function in the presence of cathode evaporation.

B. DESCRIPTION OF STANDARD RADIATION AND DIODE

In the following, the ionization of a standard diode due to the incident radiation at the surface of the core of a 5 MW reactor will be calculated. The standard diode is assumed to have a gap width of 1 mm filled with Xe at a pressure of 250 torr bounded by molybdenum electrodes. The standard reactor radiation is taken to be

Gammas:

$T\gamma = 10^9$ rad/hr at the core face,

or the spectrum

1 Mev – 5×10^7 photons/cm^2 sec watt
3 " – 5×10^6 "
5 " – 7.5×10^5 "
7 " – 2.2×10^5 "

Neutrons:

in the core
fast, 1 Mev – 1×10^{14} n/cm^2 sec
slow, 1 Mev – 2×10^{13} n/cm^2 sec
at the face of core
fast, – 2×10^{13} n/cm^2 sec

C. IONIZATION IN THE GAP

Some of the background necessary for the understanding of the interaction of γ-radiation with matter will now be given.

The problem of finding the ionization in the Xe of the interelectrode gap of the thermionic diode can be divided into two parts: 1. Direct photon-Xe interactions are possible, leading to a Xe-ion, a fast electron and, depending on the type of interaction, a photon of degraded energy. 2. It is also possible that electrons produced by the incident γ-radiation in both electrodes enter the interelectrode gap to ionize in electron-neutral collisions. Since the electron-neutral collisions generally have a greater cross section than that of direct photon-electron interactions and since the range of the energetic electrons in the material of the electrodes is of the order of mm's, the effect of such an exchange layer, e.g., electrons entering the gap from the inside of the electrodes, must be considered.

In general, the ionization in matter by incident photons is governed by an equation of the following type

$$D = A[\tau E + \delta E + \kappa(E - 2m_e c^2)], \tag{22a}$$

where D is the dose rate in Roentgen units; E is the energy of the incident photon; τ, δ, and κ are the photo-electric, Compton, and pair production adsorption coefficients, respectively; A is a conversion factor; and the term in brackets is the energy absorped per unit length of the material. Limiting ourselves to $E \leq 2m_e c^2 = 1.16$ Mev, ionization due to pair production will not be taken into account.

In Eq. (22a), only the first interaction of the primary γ-radiation of energy E has been considered. This is correct in the case of the photoelectric effect, which can be taken to be the collision of a photon with a bound electron. The total energy of the photon primary will be absorbed in one event, and the kinetic energy T of the electron produced will be determined by the excess of the photon energy beyond the binding energy Φ of the electron

$$T = E - \Phi \tag{22b}$$

However, in Compton collisions, that is, the interaction of a primary photon with a free or loosely bound electron, only a fraction of the photon energy is absorbed. A scattered photon with degraded energy is produced which in turn will interact. In absorption calculations based on the individual interaction events, such scattering of energy into the region under consideration is taken into account by the use of a buildup factor, which can amount to many times the ionization due to the primary photons.

Due to the specific geometry of the diode, a different approach can be chosen which takes into account more easily the effect of the secondary electron flux and the buildup factor due to the material boundaries of the Xe-filled gap. According to a theory by Bragg[30] and later on, by Gray,[31] the introduction of a small gas-filled cavity into a solid medium traversed by secondary electrons does not change the angular or energy distribution of the secondary electrons at the cavity location.

The conditions for the validity of the Bragg-Gray theory are:

1. Only a small fraction of the secondary electron energy is absorbed in the cavity.
2. Direct absorption of the primary radiation in the cavity is small relative to the absorbed secondary flux.
3. The cavity is surrounded by an << equilibrium >> thickness of solid, e.g., approximately equal to the range of the maximum energy secondaries.
4. The energy dissipation of the ionizing particles is uniform throughout the solid immediately surrounding the gas filled cavity.

When these conditions are fulfilled, as they are in the diode under consideration, the ratio of energy lost by an electron traversing unit mass per cm^2 in the solid E_s to the energy loss in the gas E_g is equal to the ratio of the mass stopping powers of the solid S_s to the gas S_g.

$$E_s = \frac{S_s}{S_g} E_g. \tag{23}$$

The energy loss to the gas results in ionization of the gas and can be expressed by $J_g \mathbb{W}$, where J_g is the number of ions produced per unit mass and $\mathbb{W}$ the energy necessary to produce an ion-electron pair in the gas. The ion number J_g produced per unit mass can then be expressed

$$J_g = \frac{E_s}{\mathbb{W}} \frac{S_g}{S_s}. \tag{24}$$

The mass stopping power ratio S_g/S_s can be written in terms of stopping power per electron

$$S_g/S_s = \frac{n_g}{n_s} \frac{{}_eS_g}{{}_eS_s} \tag{25}$$

where the n_s, n_g are the number of electrons per gram, and ${}_eS_s$ and ${}_eS_g$ are the stopping power $(dT/dx)_s$ and $(dT/dx)_g$, per electron, respectively.

The electron stopping powers have been calculated before by means of the Bethe-Bloch equations for the energy loss of electrons in matter and ${}_eS_g/{}_eS_s$ is taken to be 1.25. We can then write

$$J_g = 1.25 \frac{n_g}{n_s} \frac{E_s}{W} \text{ ions/g} \tag{26}$$

or the number of ions/cm^3, N, by multiplying with the mass density d in g/cm^3 where $d = n_{xe} A_{xe}$ (n_{xe} = Number of Xe atoms per cm^3 of diode gap and A_{xe} the mass of the atom)

$$N = 1.25 \frac{n_g}{n_s} \frac{E_s}{W} d. \tag{27}$$

E_s, the energy absorbed in the solid, is found from

$$E_s = R \times \frac{(\mu_a/\rho) \text{ solid}}{(\mu_a/\rho) \text{ air}} \times 83.8 \text{ [erg/gr]} \tag{28}$$

where R is the total dose in Roentgens and μ_a and ρ are linear absorption coefficient and density, respectively.

For 0.5 Mev γ-radiation the ratio for both the mass absorption coefficients is 2; at 0.1 Mev it is 10. Using 2,

$$E_s = R \times 168 \text{ erg/gm} \tag{29}$$

or, for the 5 MW reactor, assuming R (Roentgen) and rad to be equal

$$E_s = 840 \text{ erg/gm} \tag{30}$$

and the number of ions produced per unit diode area is found to be

$$n_+ = 1.2 \times 10^{15} \text{ ions/cm}^2 \text{ sec} \tag{31}$$

for a diode of 1-mm gap and 250-torr Xe pressure.

A similar contribution is added by the neutron flux, so that a good value for the ions produced by the total radiation flux is given by

$$n_+ = 2 \times 10^{15} \text{ ions/cm}^2 \text{ sec} \tag{32}$$

There is an additional correction that must be used. Experimental checks of the Bragg-Gray theory have given correct results, at the low atomic numbers, but greater ionization than that expected from theory for denser wall materials.[32] It appears that a conservative correction factor of 2 is indicated. Therefore, the expected value is given as

$$n_+ = 4 \times 10^{15} \text{ ions/cm}^2 \text{ sec.} \tag{33}$$

D. ION PRODUCTION RATE IN CESIUM PLASMA

An approximate value of the ion production rate in the cesium plasma of the arc mode thermionic energy converter is obtained by assuming a Langmuir double sheath at the cathode. Thus, the ion current density is about 1/500 times the electron current density. Thus, the ion loss rate from the plasma is

$$n_+ = \frac{j_e}{500\ e} = 1.25 \times 10^{16}\ j_e \text{ ions/cm}^2/\text{sec} \tag{34}$$

where j_e = electron current density in A/cm^2 and e = electronic charge. Due to the density gradient the ion losses to the anode can be neglected. At a representative current density of 4 A/cm^2 the ion production rate becomes

$$n_+ = 5 \times 10^{16} \text{ ions/cm}^2/\text{sec} \tag{35}$$

Comparison with the ion generated in the xenon gas at the 5-MW reactor level shows that it is about 10 percent of the cesium ion generation rate at the assumed current density. This is large enough to be observed in an experiment. Since the Xe ions are generated uniformly throughout the diode space their effect on converter output may be higher than the numbers seem to indicate.

E. CONCLUSIONS

At a 5-MW reactor average power density level the effect of xenon dosing a thermionic converter may give a measurable improvement in converter output. Because of the uncertainties in ion production rate and its effect on converter performance an experimental investigation is essential. The secondary effects of ionization of the xenon gas by the reactor fluxes, such as automatic diode ignition and increased plasma stability, would seem to be important enough by themselves to justify an experimental investigation.

REFERENCES

1. J. D. Levine and E. P. Gyftopoulos, J. Appl. Phys. **33**, 67 (1962).
2. J. D. Levine and E. P. Gyftopoulos, "Adsorption Physics of Metallic Particles. Part I: Atom and Ion Desorption Energies, " to be published in Journal of Surface Science (1964).
3. J. D. Levine and E. P. Gyftopoulos, "Adsorption Physics of Metallic Particles. Part II: Desorption Rates of Atoms and Ions," to be published in Journal of Surface Science (1964).
4. J. D. Levine and E. P. Gyftopoulos, "Adsorption Physics of Metallic Particles. Part III: Equations of State Hysteresis Effects and Electron Emission S-Curves," to be published in Journal of Surface Science (1964).
5. N. S. Rasor and C. Warner III, "Atomics International First Summary Report of Basic Research in Thermionic Energy Conversion Processes," p. 45, Nov. 1961 – AI-6799.
6. J. B. Taylor and I. Langmuir, Phys. Rev. **44**, 423 (1933).
7. W. E. Danforth, J. Appl. Phys. **33**, 1972 (1962).
8. E. N. Carabateas, J. Appl. Phys. **33**, 2698 (1962).
9. R. Gomer, *Field Emission and Field Ionization,* (Harvard Univ. Press, Cambridge, Mass., 1961).
10. S. T. Martin, Phys. Rev. **60**, 947 (1939).
11. H. F. Webster, J. Appl. Phys. **32**, 1802 (1961).
12. J. M. Houston and H. F. Webster, *Advances in Electronics and Electron Physics* **17**, (Academic Press, New York, 1962) p. 125.
13. R. L. Aamodt, L. J. Brown, and B. D. Nichols, "Thermionic Emission from Molybdenum IV Vapors of Cesium and Cesium Fluoride," J. Appl. Phys. **33**, 2080 (1962).
14. G. N. Hatsopoulos and S. Kitrilakis, 22nd Annual Conference on Physical Electronics, M.I.T., March (1962) p. 152.
15. J. G. de Steese, Applied Physics Letters **2**, 25 (1963).
16. J. D. Levine, Proceedings of Thermionic Specialists Conference, Gatlinburg, Tenn. IEEE October (1963).
17. I. Langmuir and K. H. Kingdon, Proc. Roy. Soc. **A107**, 61 (1925).
18. J. Becker, Am. Electrochem. Soc. Trans. **55**, 153 (1929).
19. A. J. W. Moore and H. W. Allison, J. Chem. Phys. **23**, 1609 (1955).
20. Ya. P. Zingerman and V. A. Ishchuk, Soviet Physics (Solid State) **4**, 1618 (1963). In English.
21. B. L. Blackford, Temperature Dependence of Electrical Leakage Caused by Cesium on Glass, Quarterly Progress Report No. 68 of Research Laboratory of Electronics, M.I.T. (1963) p. 2.
22. A. C. B. Lovell, Electrical Conductivity of Thin Metallic Films. Part I. Rubidium on Pyrex Glass Surface, Proc. Roy. Soc. (London) **A 157**, 311 (1936) and Part III. Alkali Films with Properties of Normal Metal, Proc. Roy. Soc. (London) **A 166**, 270 (1938).
23. E. T. S. Appleyard and A. C. B. Lovell, Part II. Cesium and Potassium on Pyrex Glass Surfaces, Proc. Roy. Soc. (London) **A 158**, 718 (1937).
24. G. A. Swartz and L. S. Napoli, Bull. Am. Phys. Soc. **7**, 150 (1962).
25. Saul Dushman and J. M. Lafferty, *Scientific Foundations of Vacuum Technique* (John Wiley and Sons, Inc., New York, 1962).

REFERENCES (Continued)

26. J. R. Young, Rev. Sci. Instr. **34**, 375 (1963), and **34**, 891 (1962).
27. G. Thomas and L. Herman, Compt. rend. **229**, 1313 (1949).
28. G. Ehrlich and F. G. Hudda, J. of Chem. Phys. **30**, 493 (1959).
29. K. G. Hernqvist and E. O. Johnson, Phys. Rev. **98**, 1576 (1955).
30. W. H. Bragg, *Studies in Radioactivity* (The Macmillan Co., New York, 1912).
31. L. H. Gray, Brit. J. Radiol. **10**, 600, 721 (1937).
32. D. V. Cormack and H. E. Johns, Radiation Research **1**, 133 (1954).
    L. V. Spencer and F. V. Attix, Radiation Research **3**, 239 (1955).
    F. H. Attix and L. De La Vergne, Radiology **63**, 853 (1954).
    Also, general reference on attenuation of γ-rays and ionization. The Attenuation of Gamma Rays and Neutrons in Reactor Shields by H. Goldstein, Div. of Reactor Development, AEC, 1957.